

Analysis of the heat flux characteristics in the helical scrape-off layer of Wendelstein 7-X start up scenarios by 3-D modeling

F. Effenberg¹, Y. Feng², H. Frerichs¹, O. Schmitz¹, T. Barbui¹, J. Geiger², M. Jakubowski², R. König², M. Krychowiak², H. Niemann², T. Sunn Pedersen², L. Stephey³, G.A. Wurden⁴, & W7-X Team

¹ Department for Engineering Physics, University of Wisconsin - Madison, Madison, WI, USA

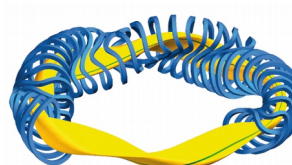
² Max-Planck-Institut für Plasmaphysik, 17491 Greifswald, Germany

³ HSX Plasma Laboratory, University of Wisconsin - Madison, Madison, WI, USA

⁴ Los Alamos National Laboratory, PO Box 1663, Los Alamos, NM 87545, USA

**58th Annual Meeting of the APS Division of Plasma Physics
October 31-November 4, 2016 • San Jose, CA**

Contact: effenberg@wisc.edu



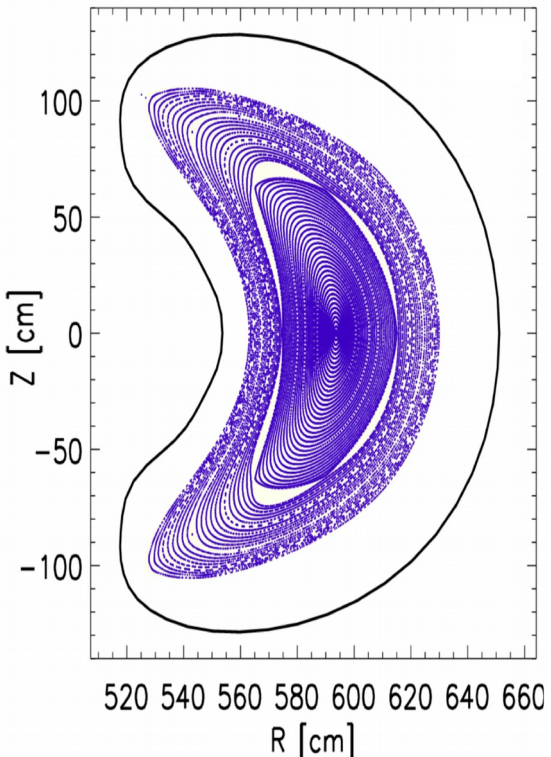
WISCONSIN
UNIVERSITY OF WISCONSIN-MADISON

Acknowledgments:

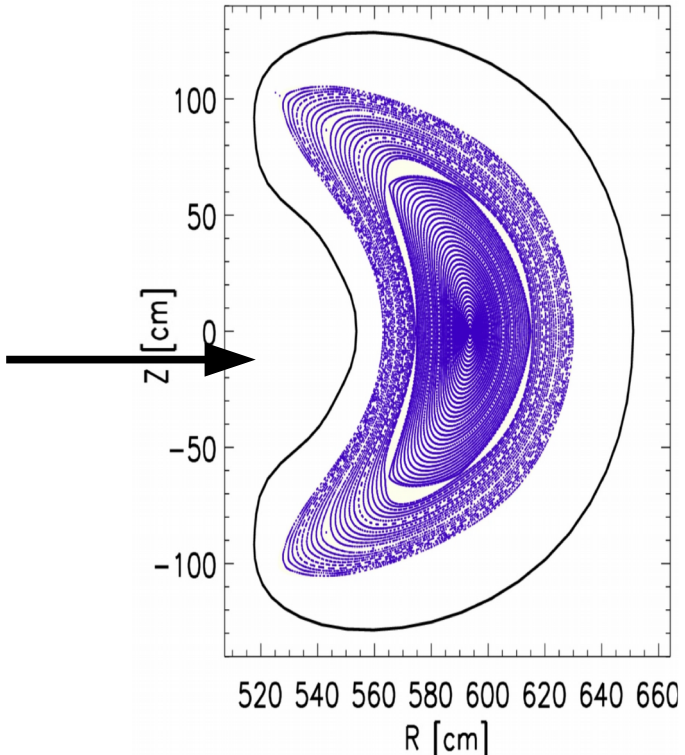
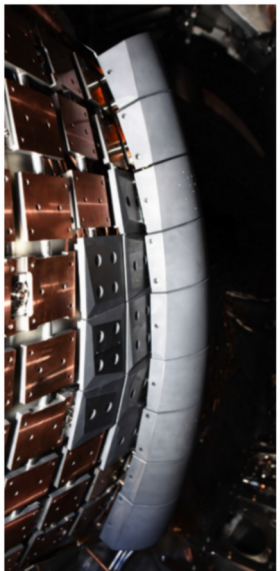
This work was supported in part by the U.S. Department of Energy (DoE) under grant DE-SC0014210 and by start up funds of the Department of Engineering Physics and of the College of Nuclear Engineering at the University of Wisconsin - Madison, USA.

This work has been carried out within the framework of the **EUROfusion Consortium** and has received funding from the **Euratom research and training programme 2014-2018** under **grant agreement No 633053**. The views and opinions expressed herein do not necessarily reflect those of the European Commission.

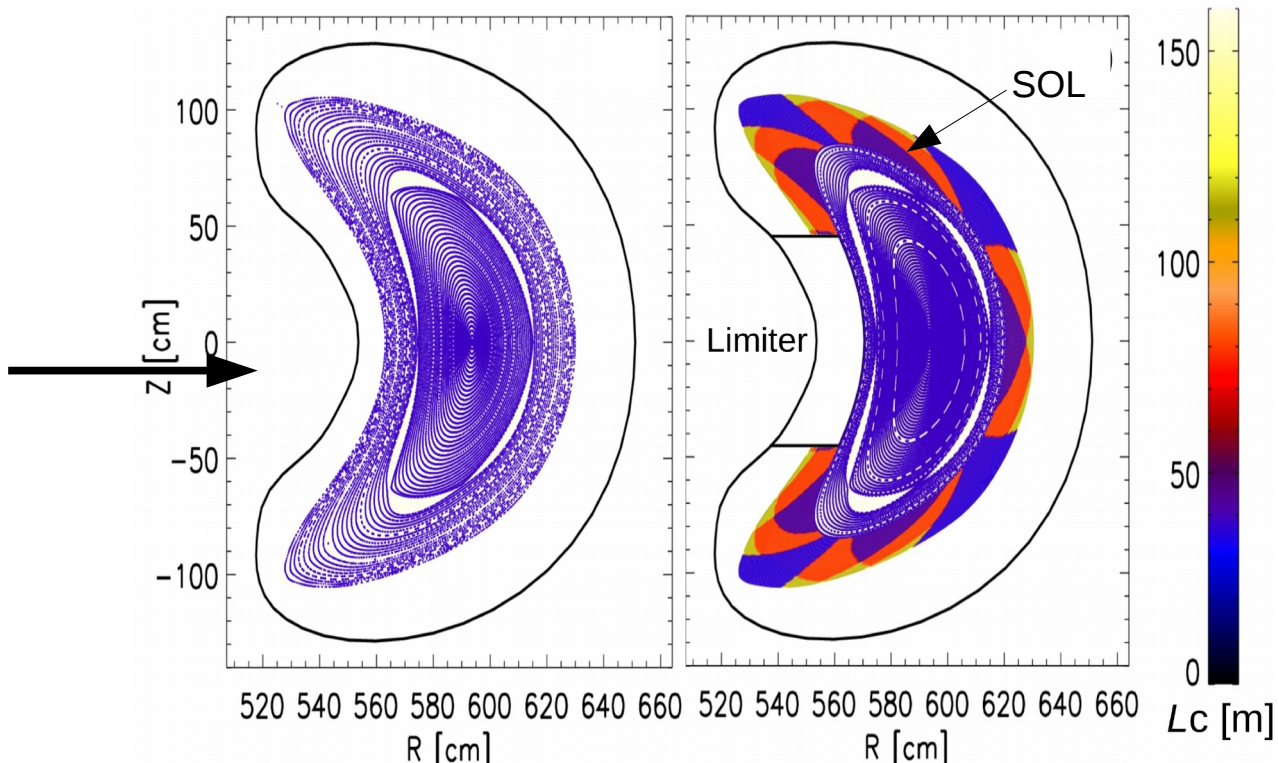
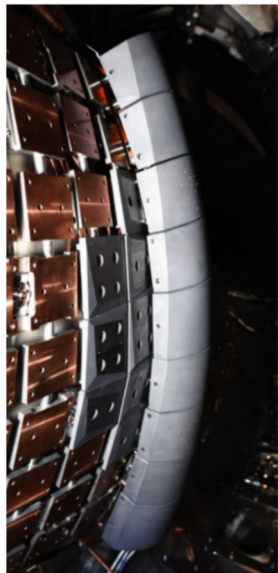
Start-up configuration: closed magnetic flux surfaces, no magnetic islands in the boundary



Start-up configuration: closed magnetic flux surfaces, no magnetic islands in the boundary

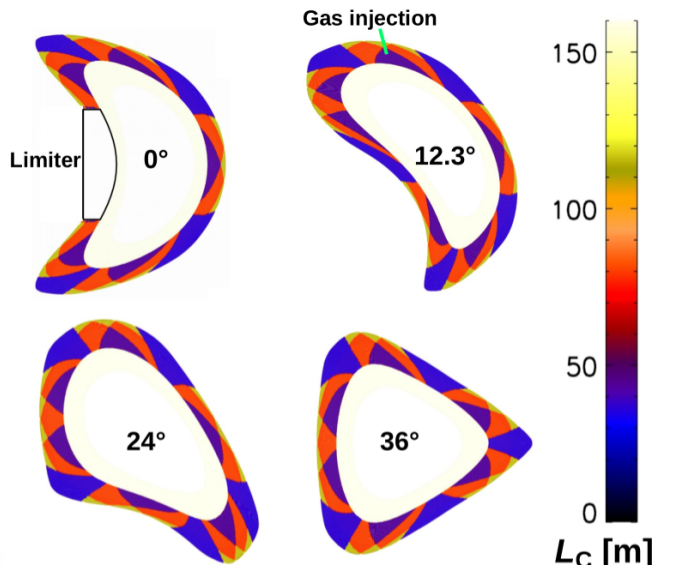


Start-up configuration: closed magnetic flux surfaces, no magnetic islands in the boundary



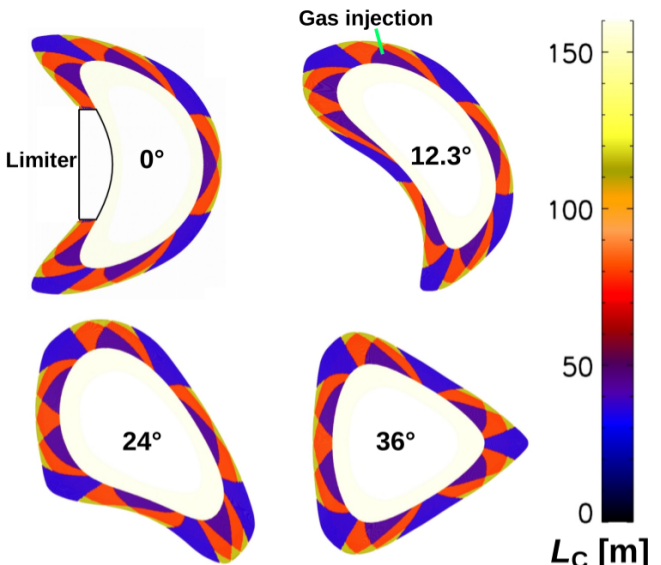
Limiters induce a 3-D helical scrape-off layer (SOL) of helical magnetic flux tubes of 3 different lengths L_c

L_c profiles show poloidal modulation

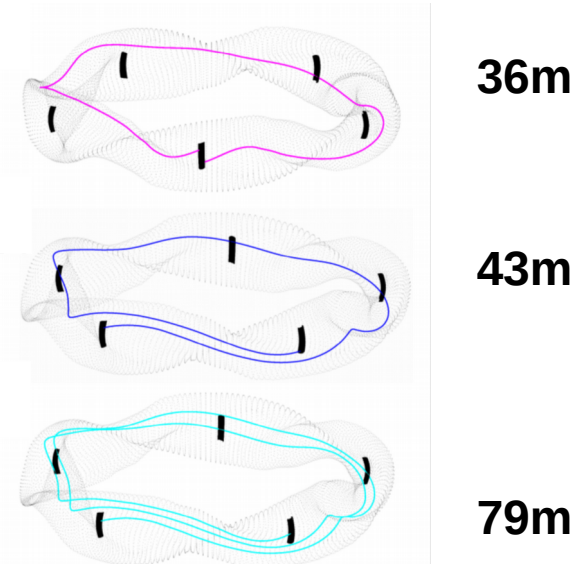


Limiters induce a 3-D helical scrape-off layer (SOL) of helical magnetic flux tubes of 3 different lengths L_c

L_c profiles show poloidal modulation

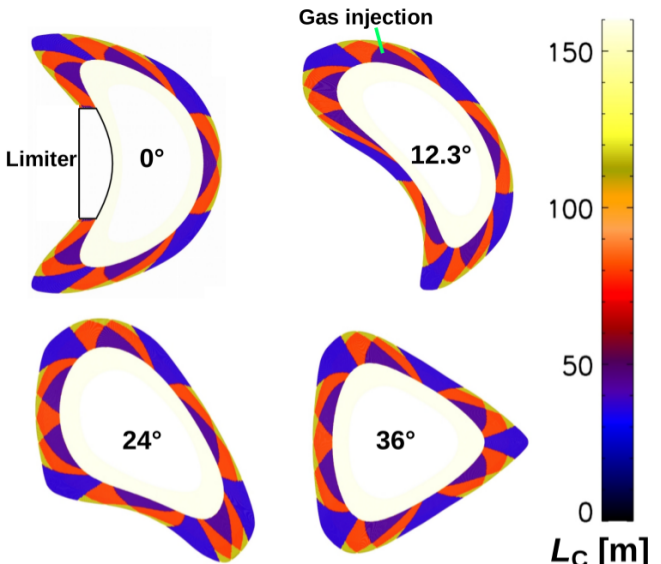


3 types of magnetic flux tubes:

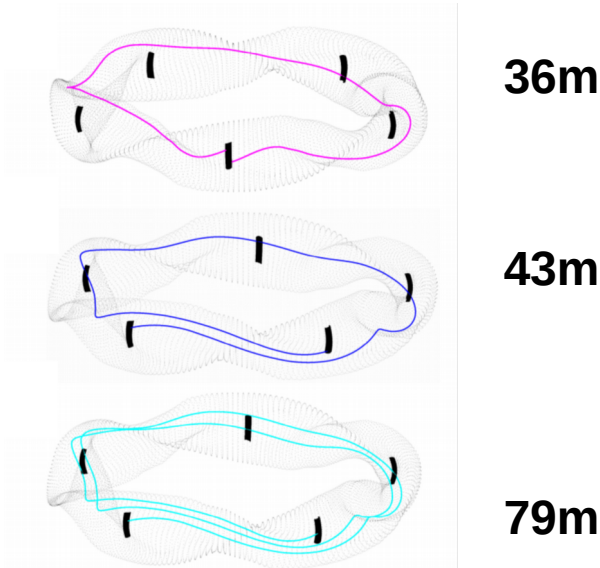


Limiters induce a 3-D helical scrape-off layer (SOL) of helical magnetic flux tubes of 3 different lengths L_c

L_c profiles show poloidal modulation

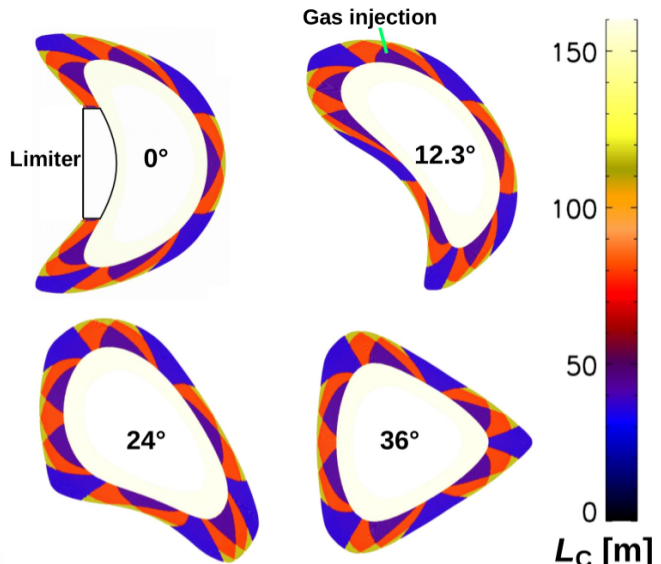


3 types of magnetic flux tubes:

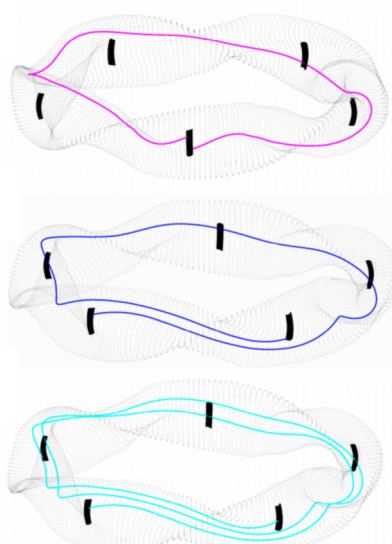


Limiters induce a 3-D helical scrape-off layer (SOL) of helical magnetic flux tubes of 3 different lengths L_c

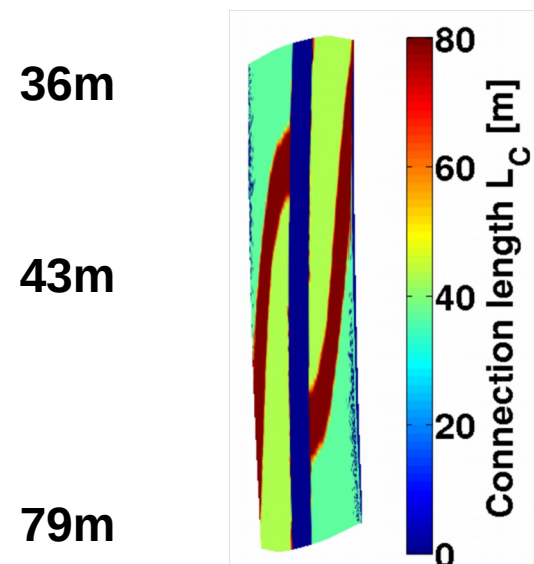
L_c profiles show poloidal modulation



3 types of magnetic flux tubes:

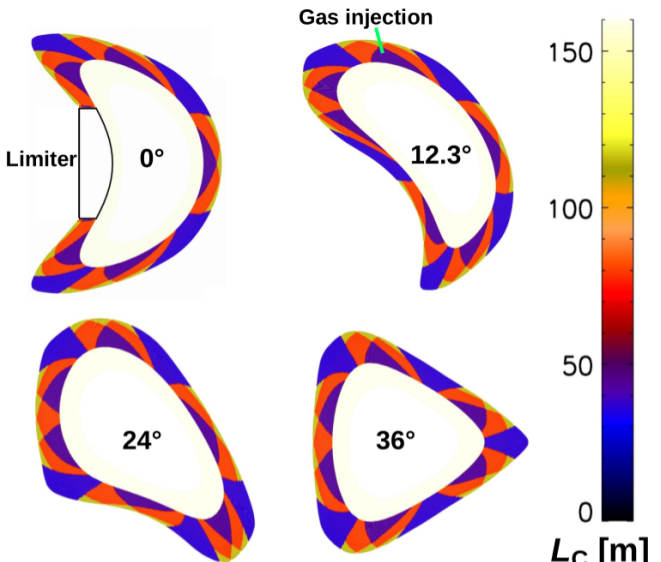


Uneven L_c distribution on limiter surface

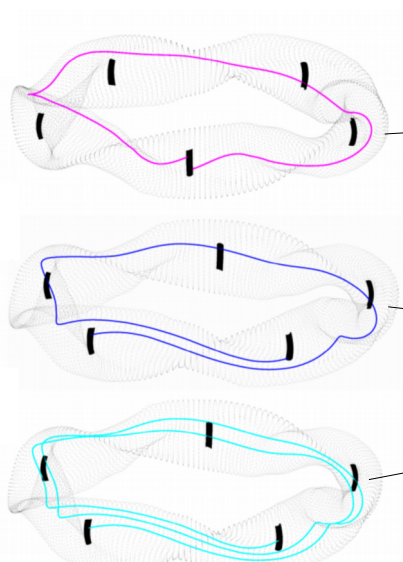


Limiters induce a 3-D helical scrape-off layer (SOL) of helical magnetic flux tubes of 3 different lengths L_c

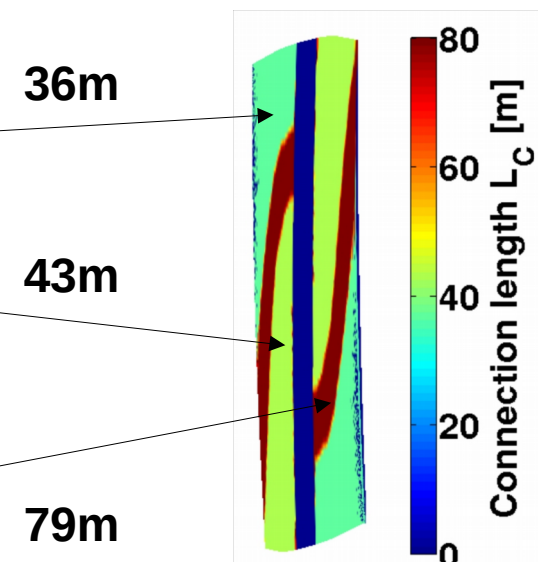
L_c profiles show poloidal modulation



3 types of magnetic flux tubes:

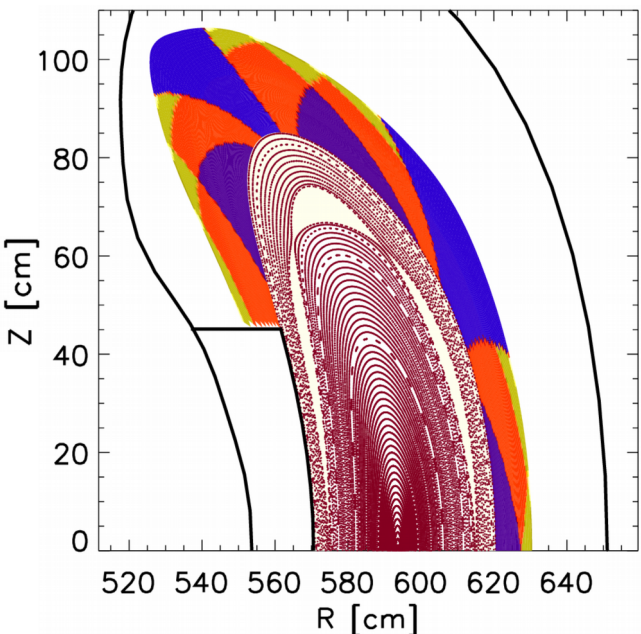


Uneven L_c distribution on limiter surface

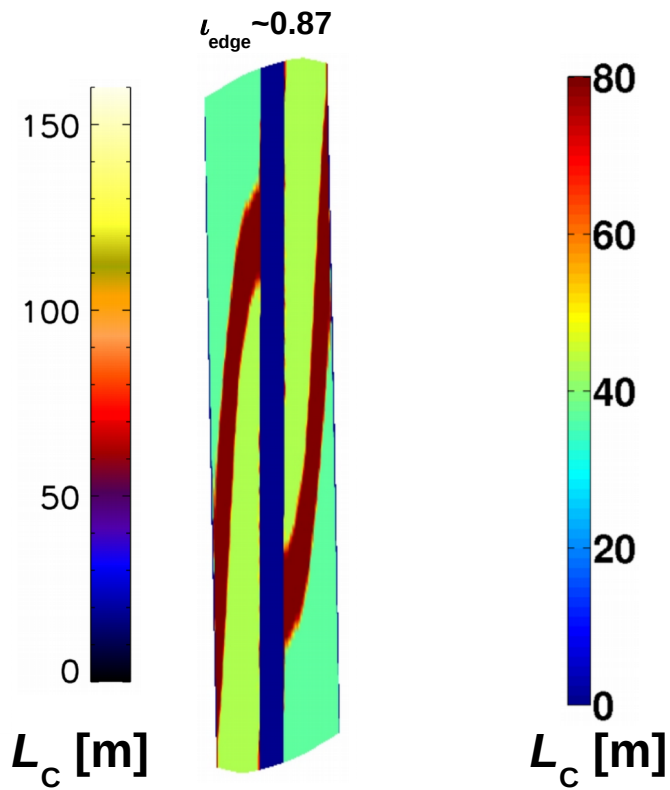


Increase of rotational transform changes SOL magnetic topology and magnetic footprint

optimized ($\iota_{\text{edge}} \sim 0.87$)

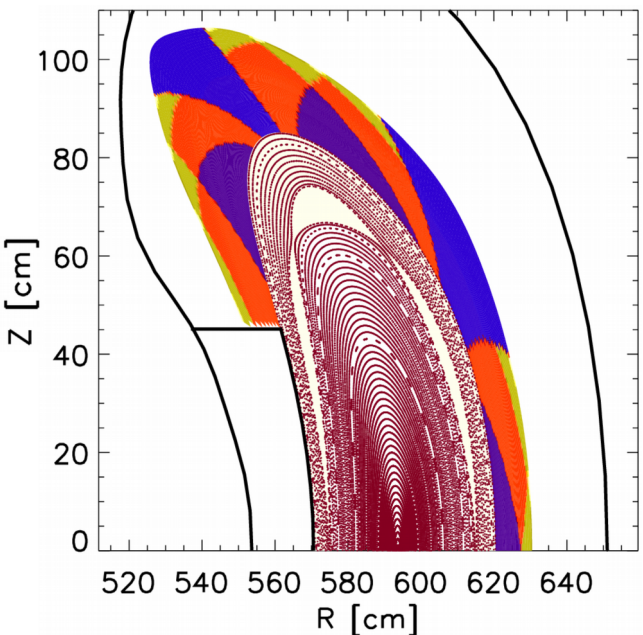


$\iota_{\text{edge}} \sim 0.87$

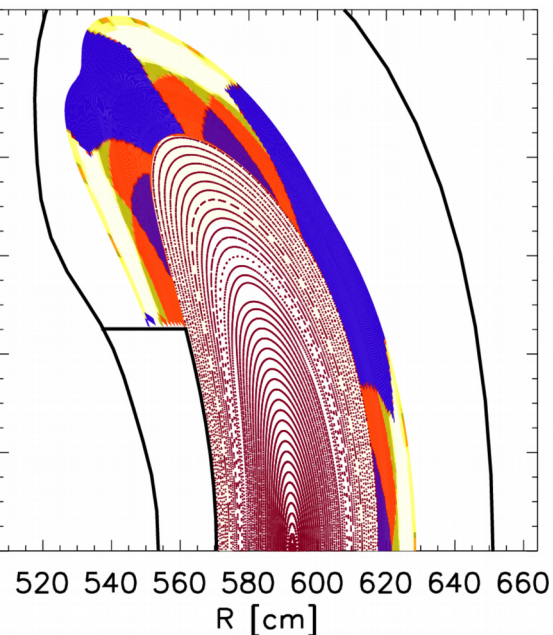


Increase of rotational transform changes SOL magnetic topology and magnetic footprint

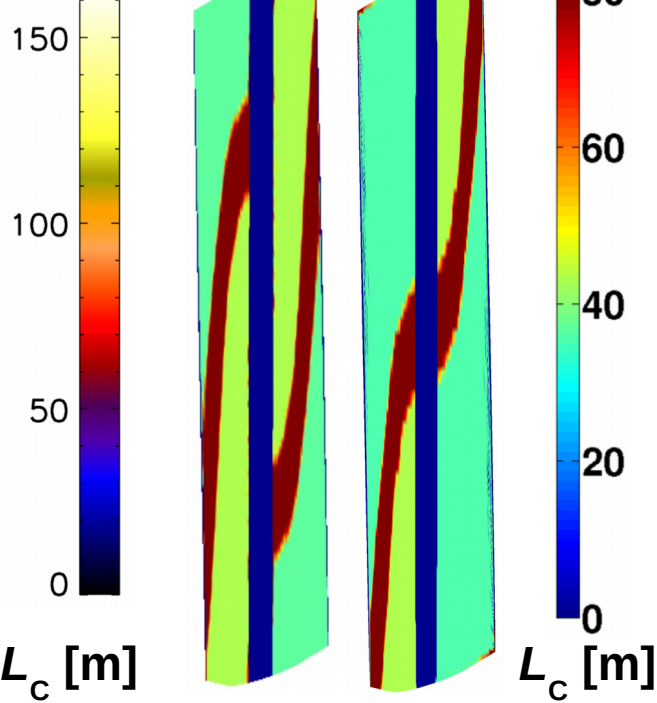
optimized ($\iota_{\text{edge}} \sim 0.87$)



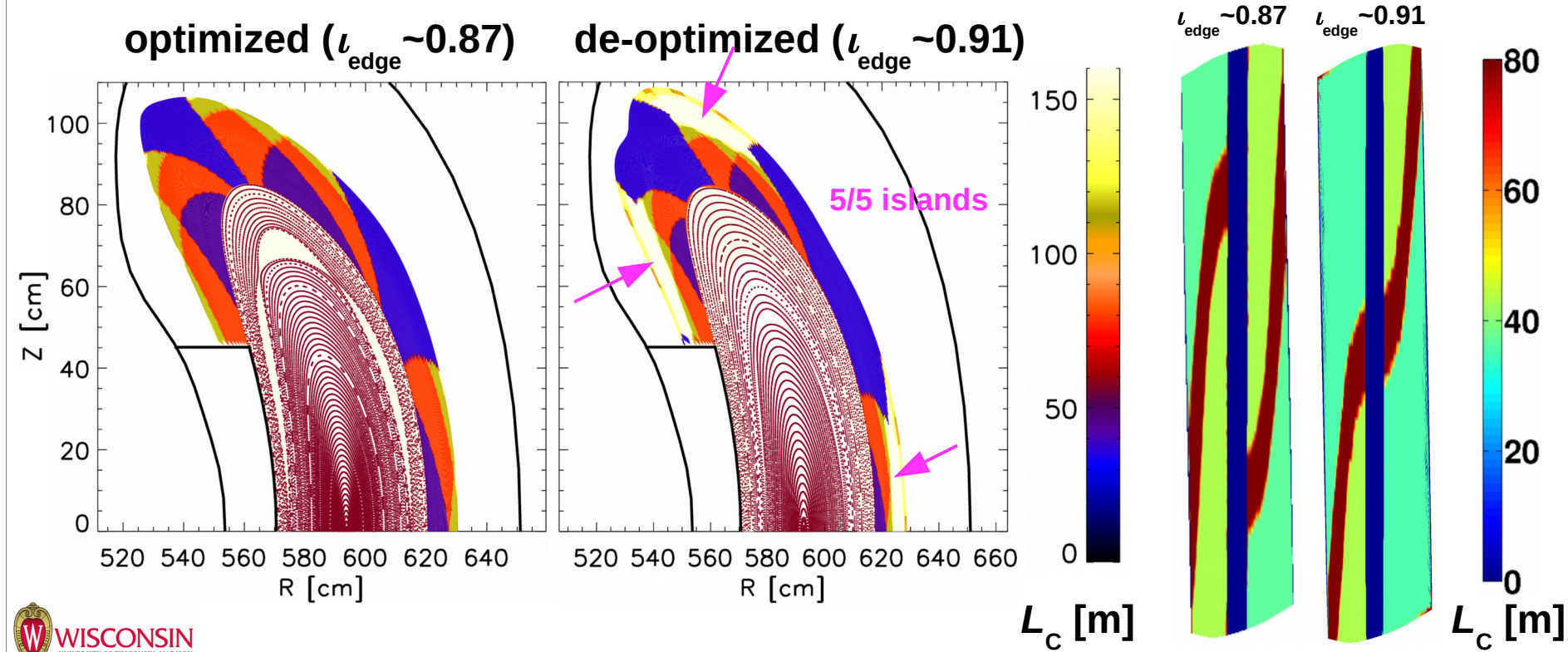
de-optimized ($\iota_{\text{edge}} \sim 0.91$)



$\iota_{\text{edge}} \sim 0.87$ $\iota_{\text{edge}} \sim 0.91$

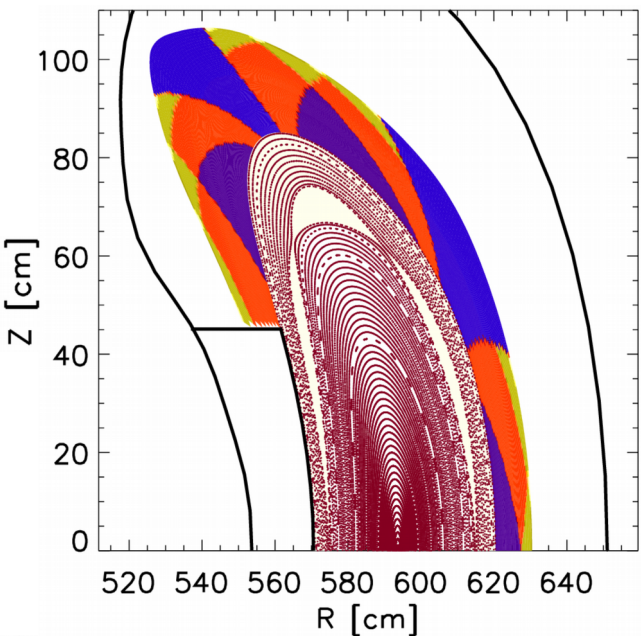


Increase of rotational transform changes SOL magnetic topology and magnetic footprint

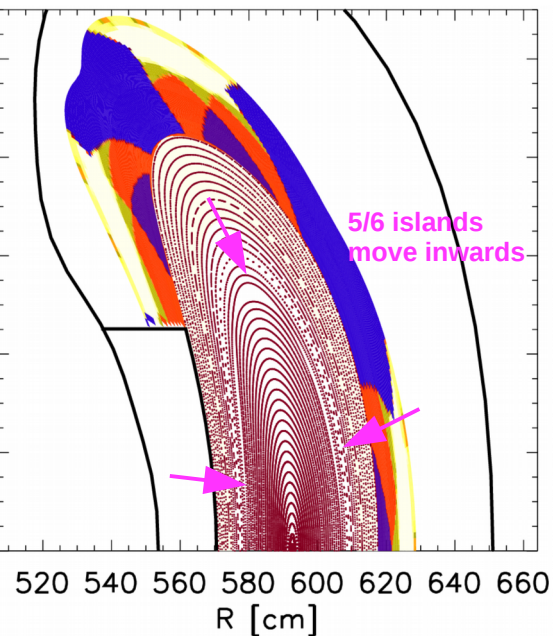


Increase of rotational transform changes SOL magnetic topology and magnetic footprint

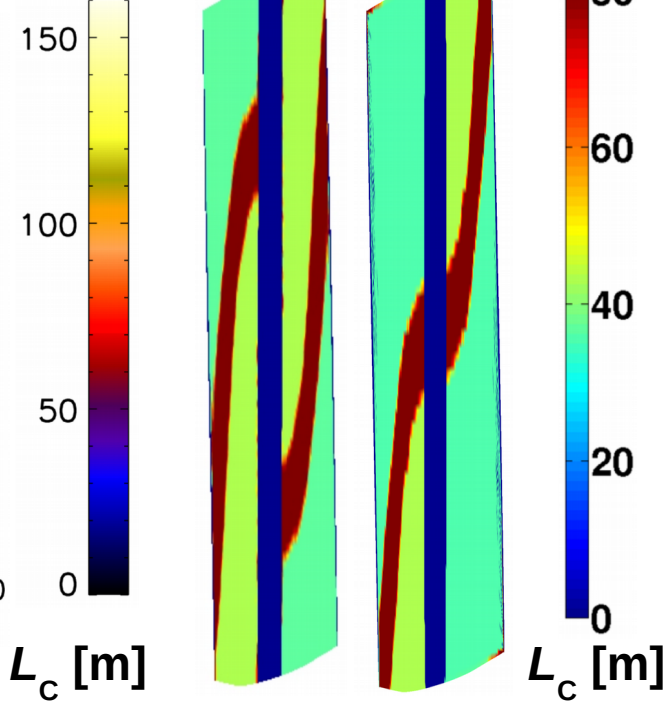
optimized ($\iota_{\text{edge}} \sim 0.87$)



de-optimized ($\iota_{\text{edge}} \sim 0.91$)

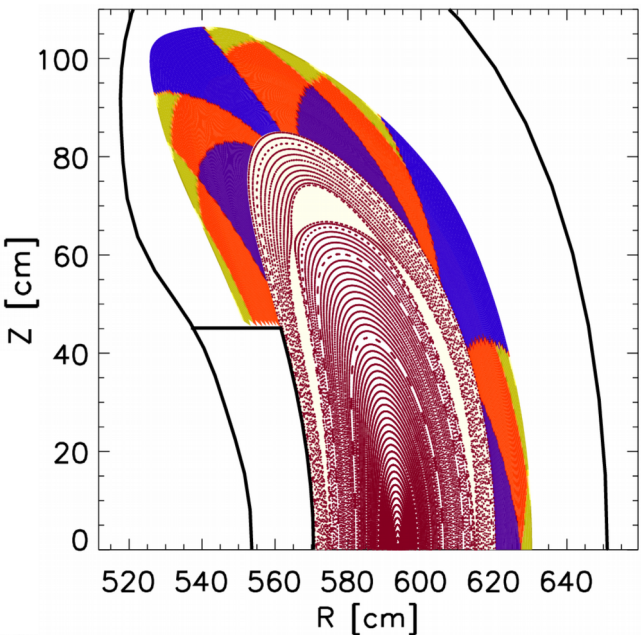


$\iota_{\text{edge}} \sim 0.87$ $\iota_{\text{edge}} \sim 0.91$

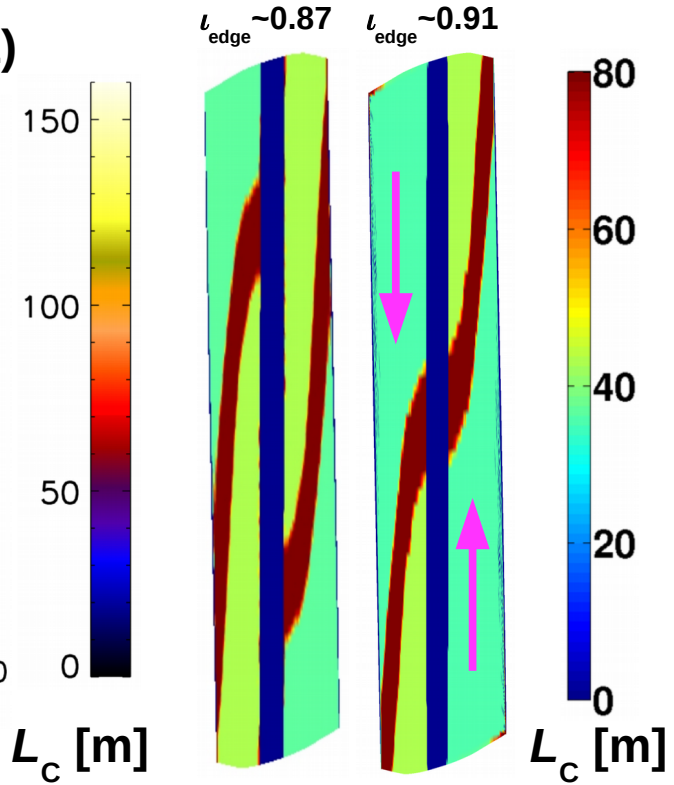
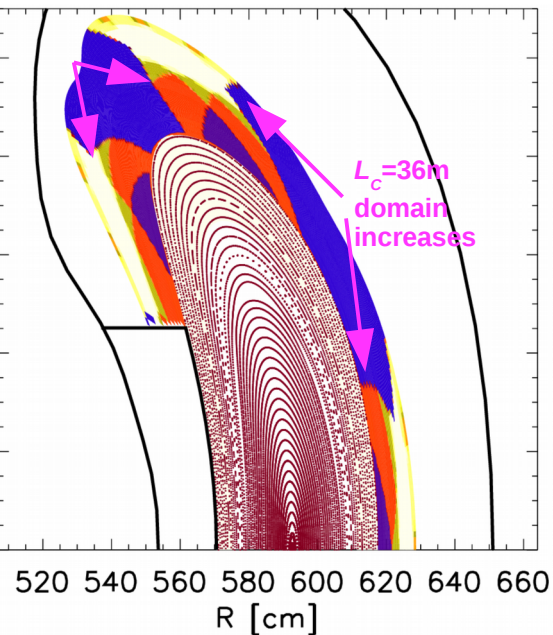


Increase of rotational transform changes SOL magnetic topology and magnetic footprint

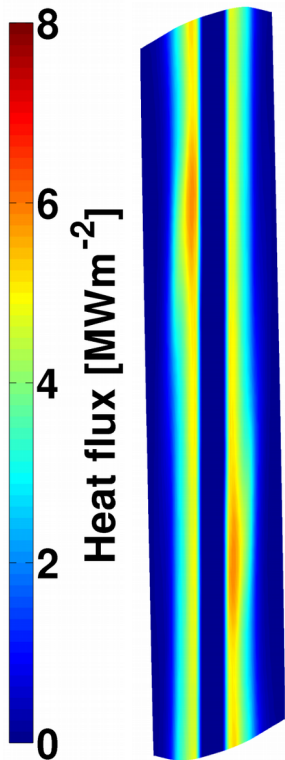
optimized ($\iota_{\text{edge}} \sim 0.87$)



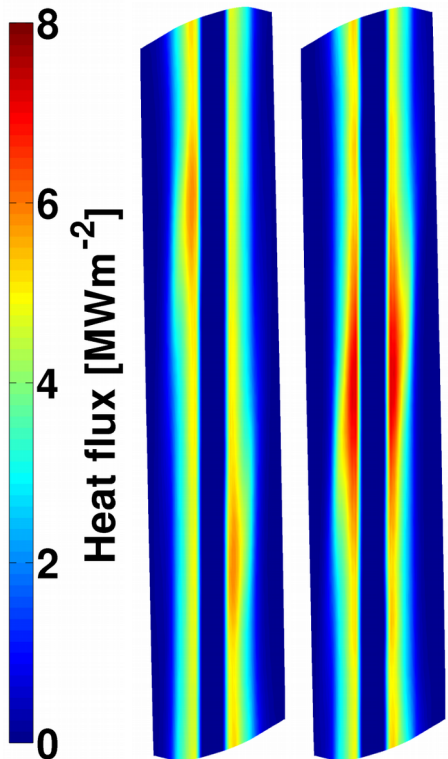
de-optimized ($\iota_{\text{edge}} \sim 0.91$)



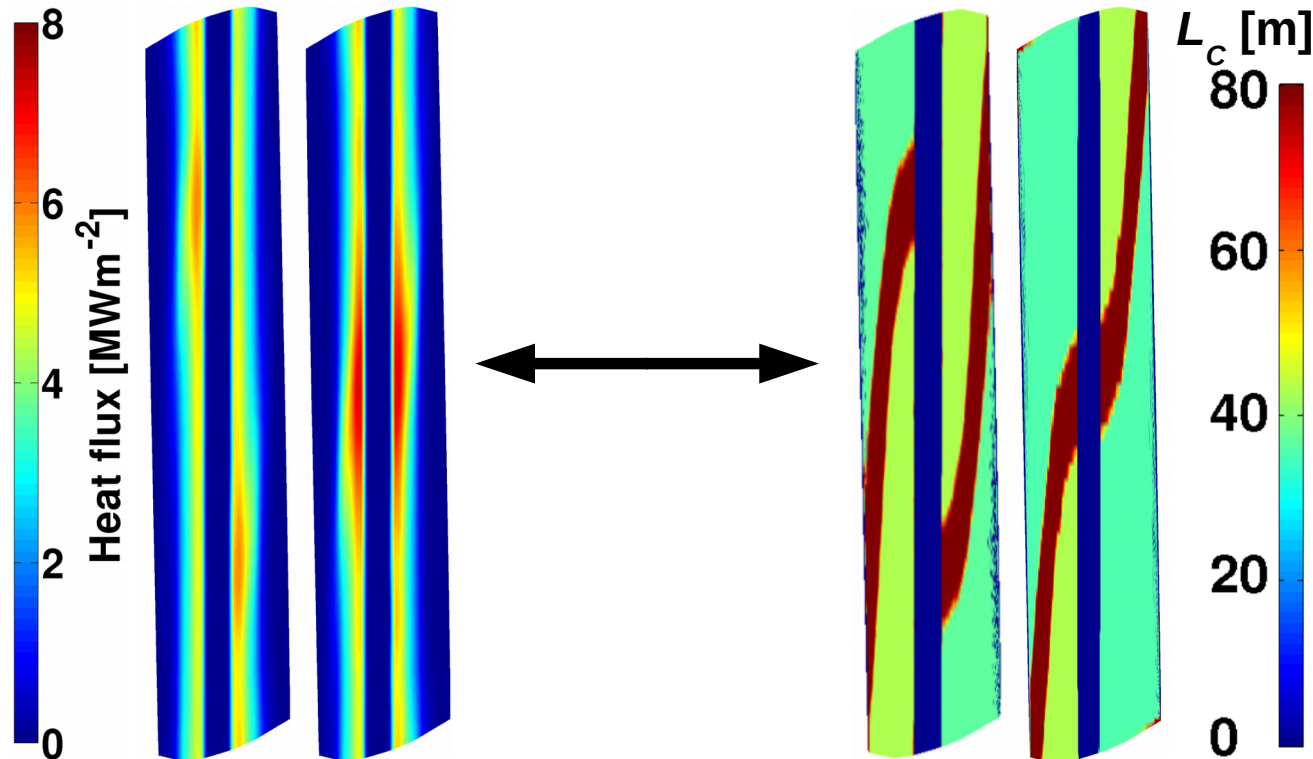
Change of rotational transform: limiter heat load patterns strongly correlated to distribution of L_c



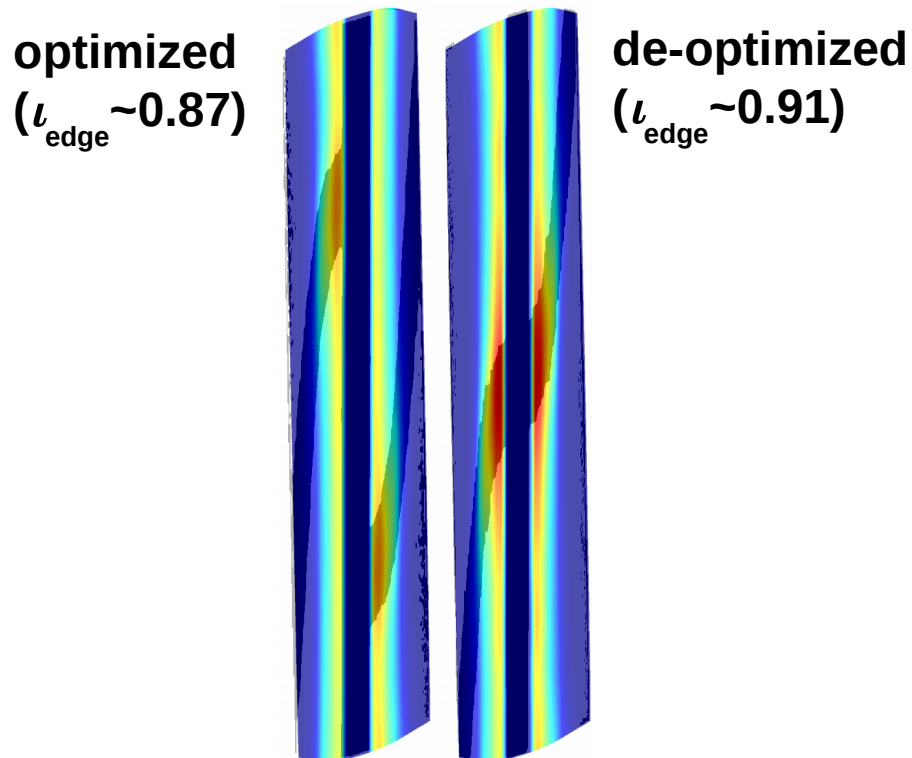
Change of rotational transform: limiter heat load patterns strongly correlated to distribution of L_c



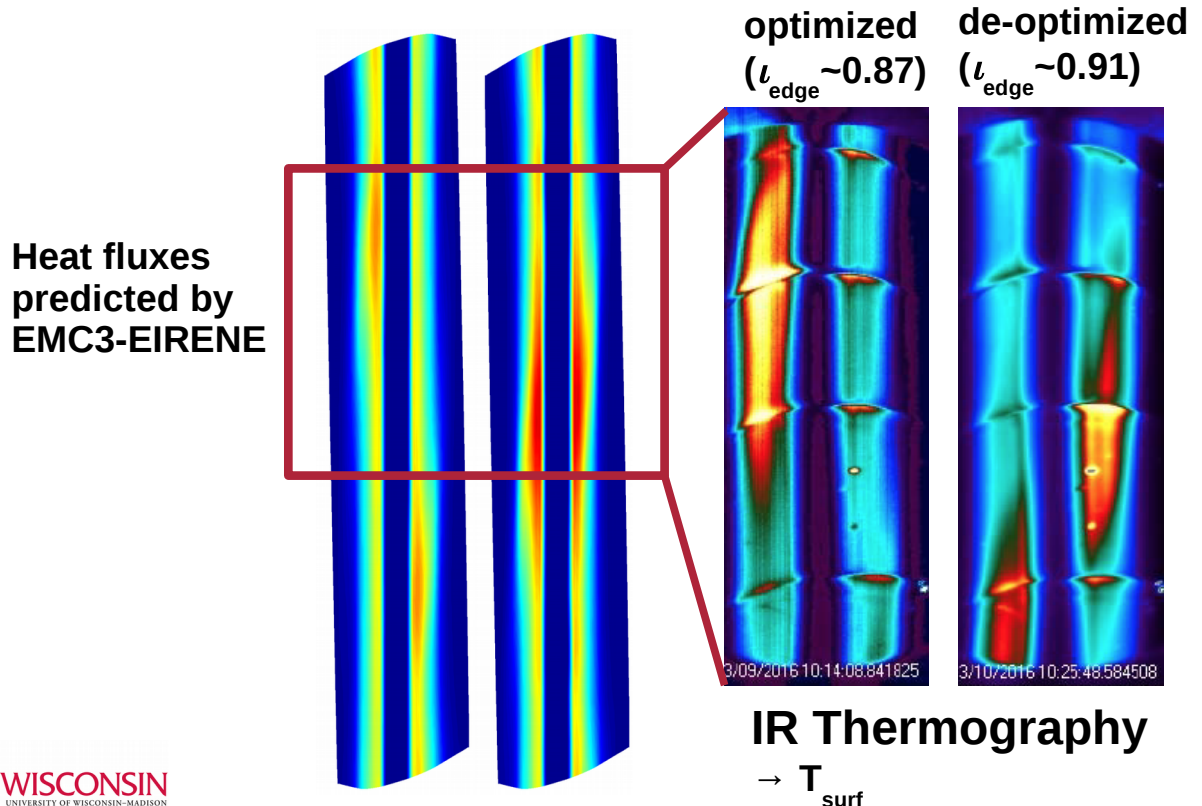
Change of rotational transform: limiter heat load patterns strongly correlated to distribution of L_c



Change of rotational transform: limiter heat load patterns strongly correlated to distribution of L_c

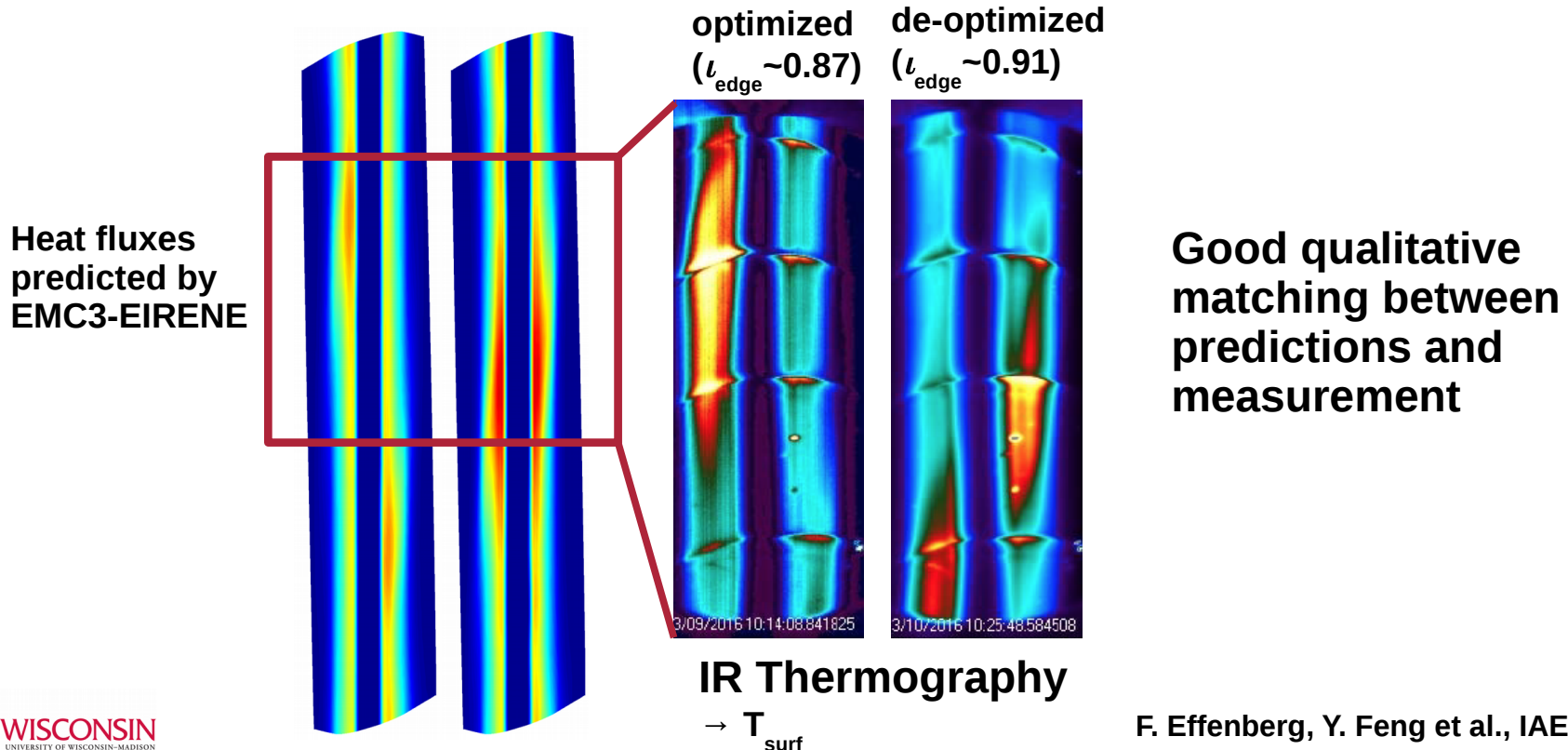


Change of rotational transform: limiter heat load patterns strongly correlated to distribution of L_c

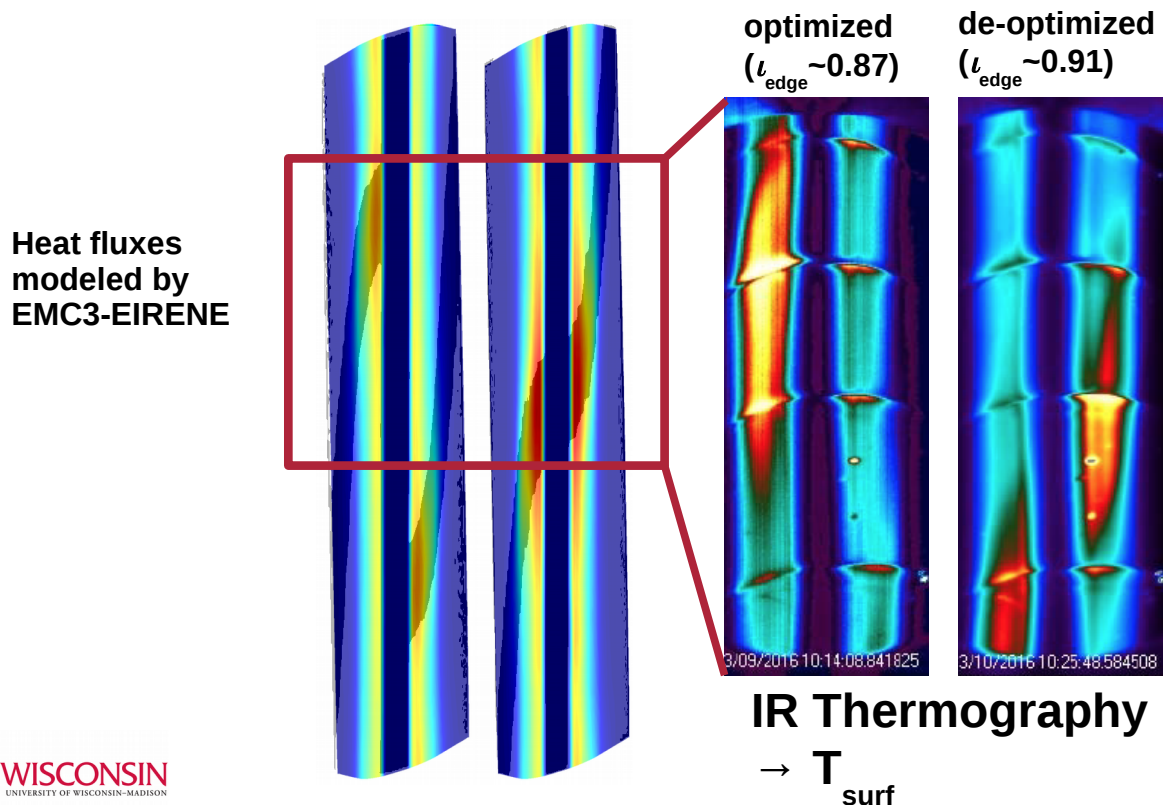


F. Effenberg, Y. Feng et al., IAEA, 2016

Change of rotational transform: limiter heat load patterns strongly correlated to distribution of L_c



Change of rotational transform: limiter heat load patterns strongly correlated to distribution of L_c



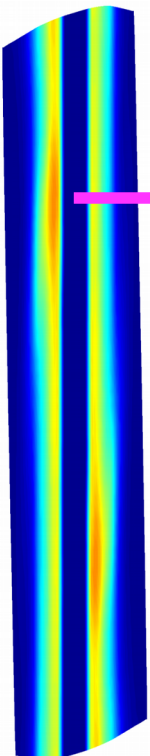
G. Wurden, H. Niemann
et al.: CP10.00054 (Mo)

H. Frerichs, F. Effenberg
et al.: TP10.00074 (Th)

V. Winters, C. Biedermann
et al.: TP10.00073 (Th)

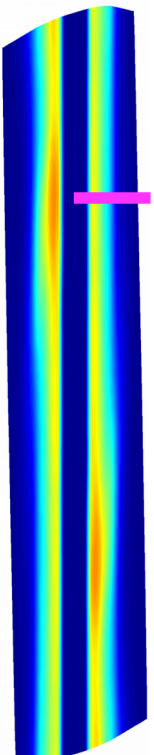
F. Effenberg, Y. Feng et al., IAEA, 2016

Heat fluxes feature different level and decay in near and far SOL and in long and short L_c



Heat fluxes feature different level and decay in near and far SOL and in long and short L_c

Heat fluxes
modeled by
EMC3-EIRENE

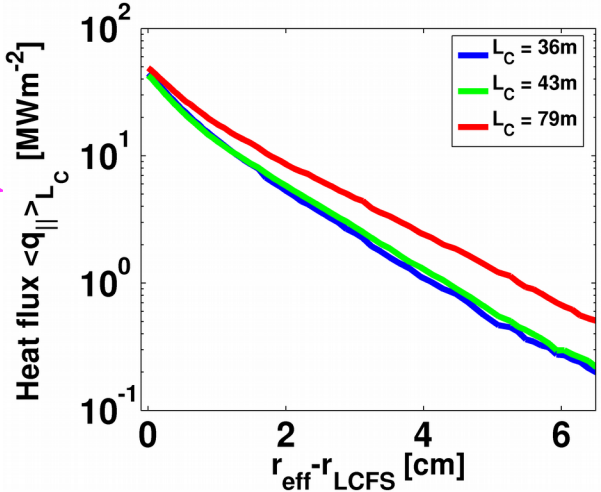
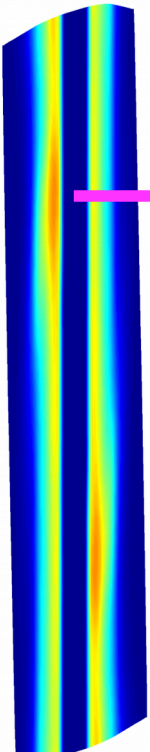


$$q_{||}$$

$$\begin{aligned} & q_{||Lc=36m} \\ & q_{||Lc=43m} \\ & q_{||Lc=79m} \end{aligned}$$

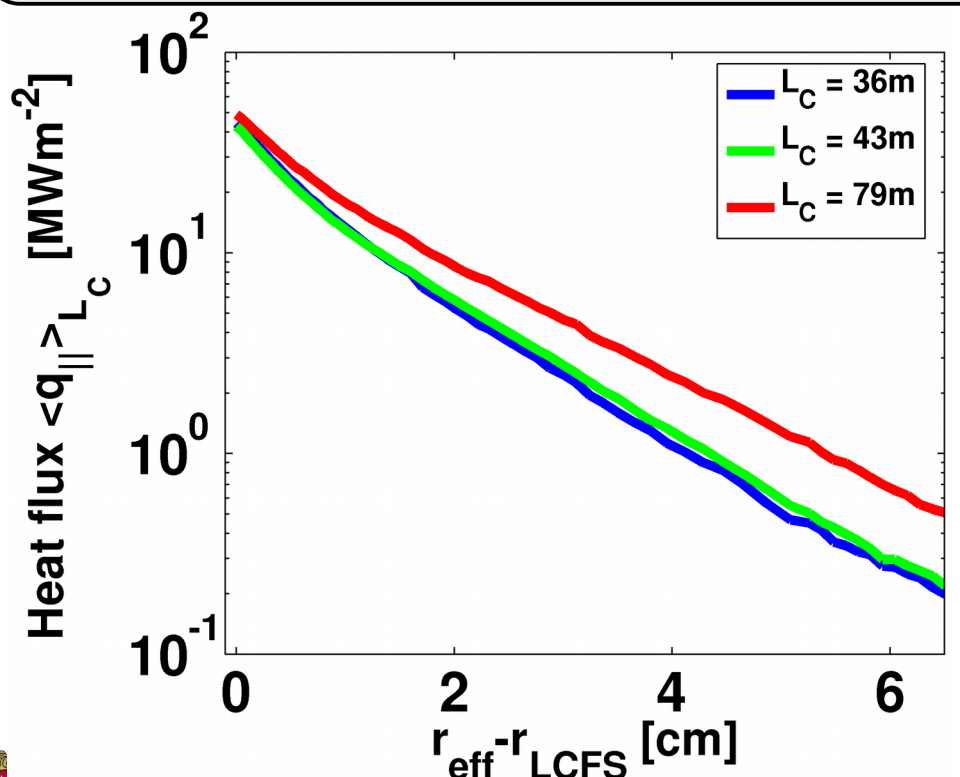
Heat fluxes feature different level and decay in near and far SOL and in long and short L_c

Heat fluxes modeled by EMC3-EIRENE

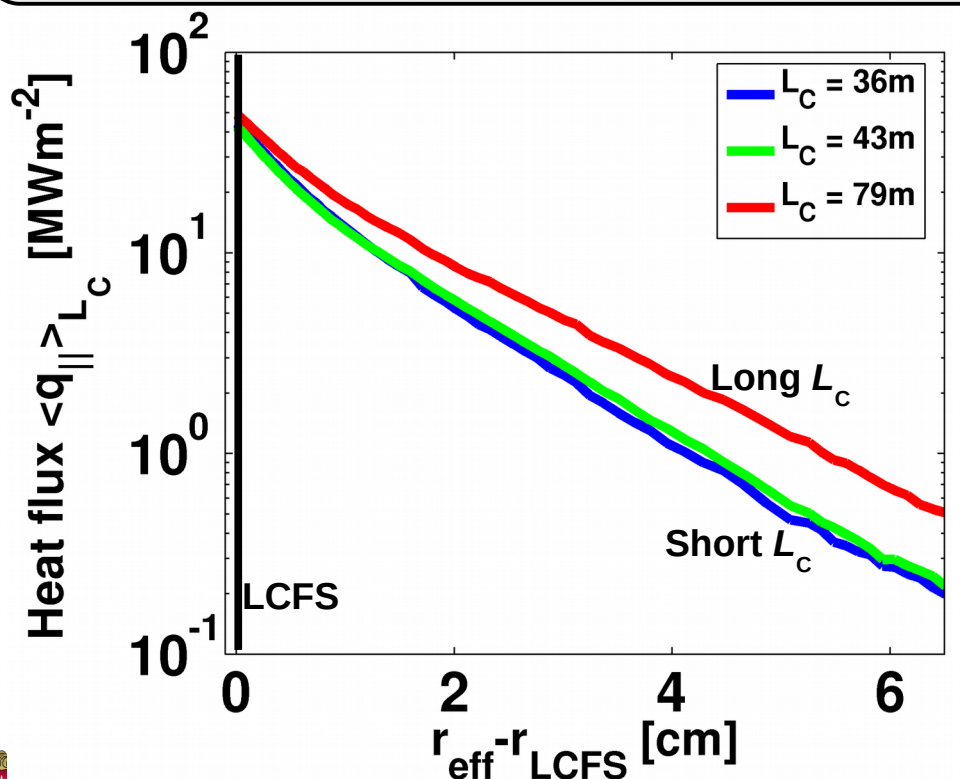


Get radial heat flux profiles (averaged in L_c)

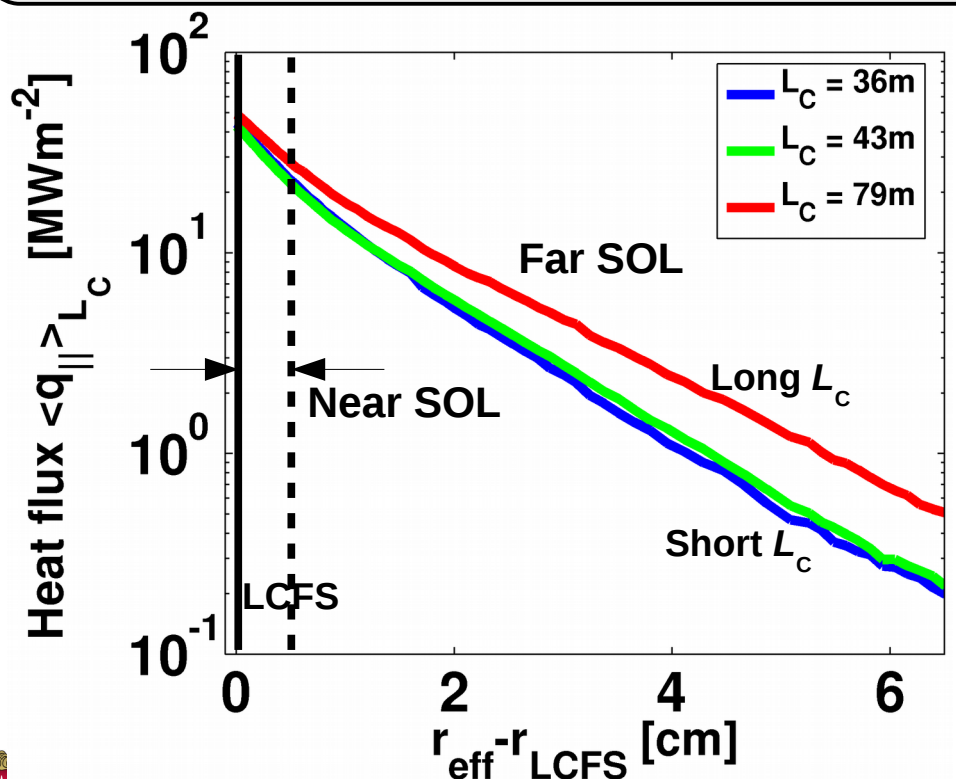
Near and far SOL identified in heat flux profile with dependence of heat flux on L_c



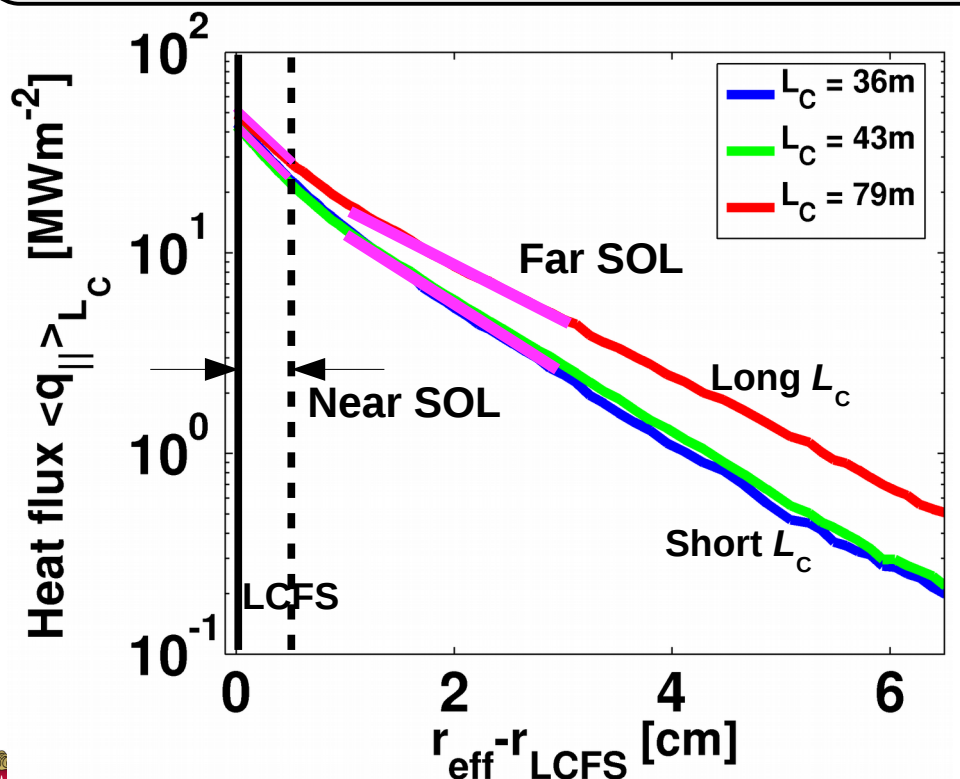
Near and far SOL identified in heat flux profile with dependence of heat flux on L_c



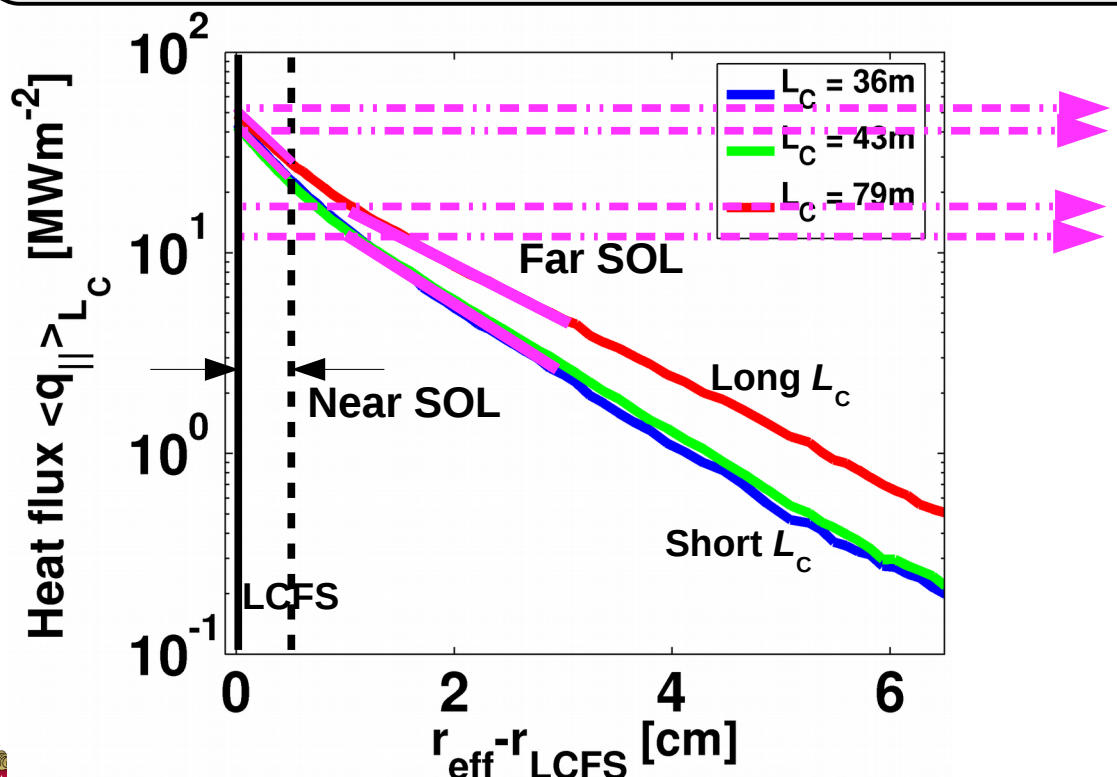
Near and far SOL identified in heat flux profile with dependence of heat flux on L_c



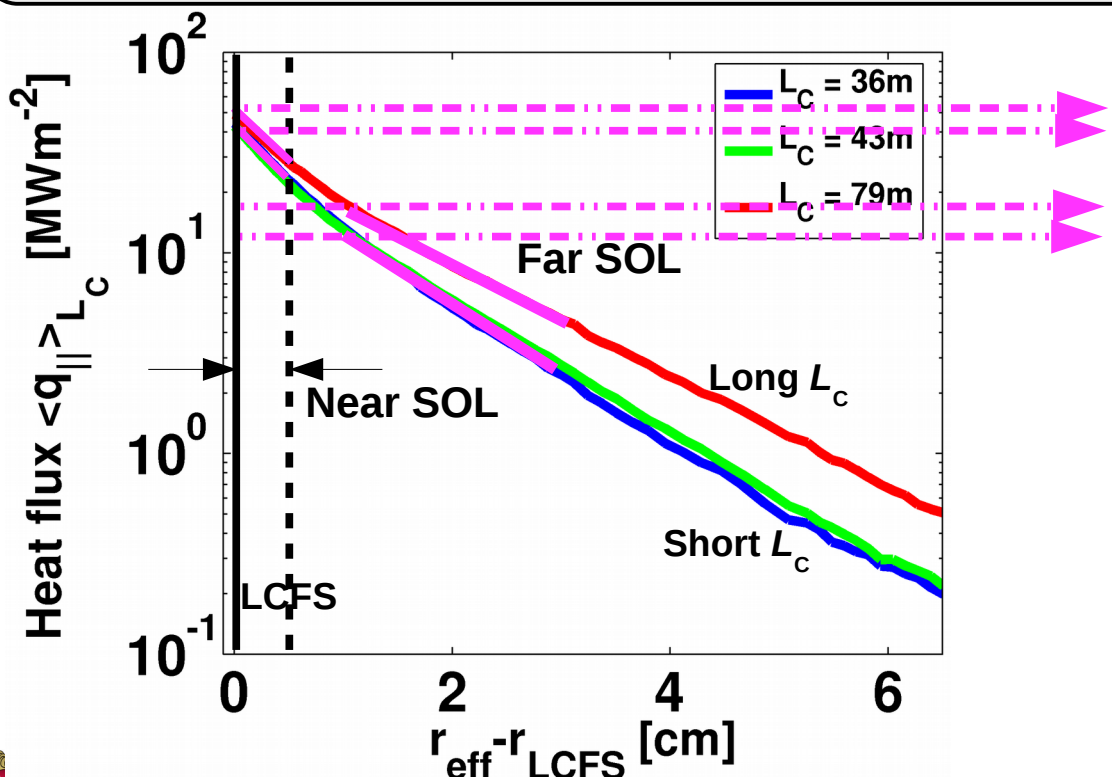
Near and far SOL identified in heat flux profile with dependence of heat flux on L_c



Near and far SOL identified in heat flux profile with dependence of heat flux on L_c

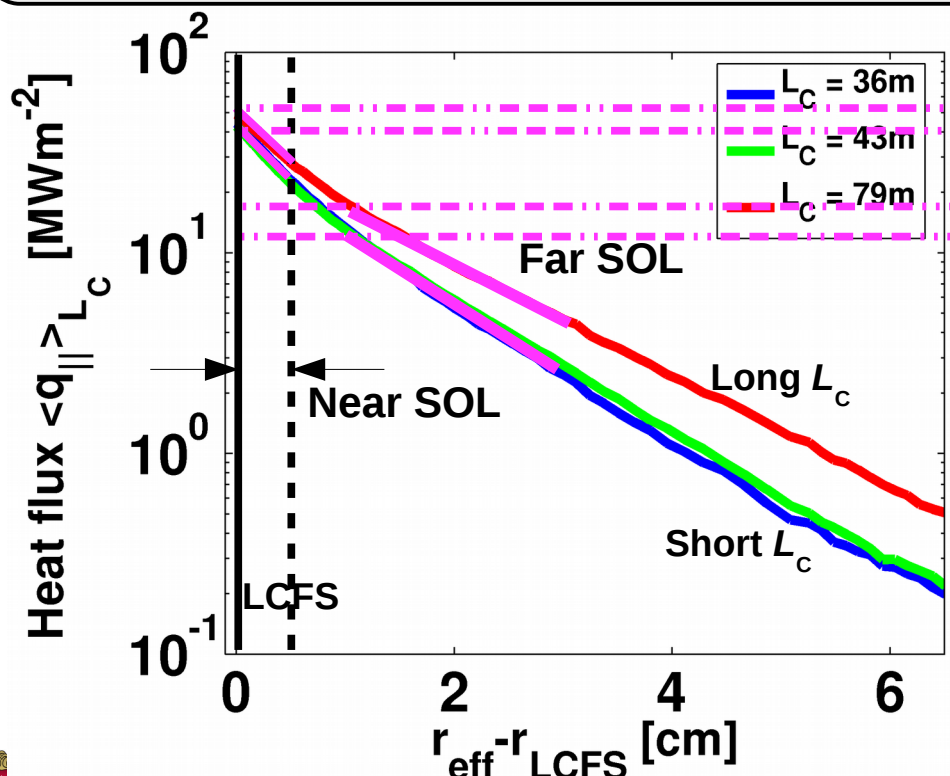


Near and far SOL identified in heat flux profile with dependence of heat flux on L_c



Heat flux characteristics
($\lambda_{q_{\parallel},\text{near,far}}$, $q_{\text{peak,near,far}}$) for
near and far SOL for
long and short L_c

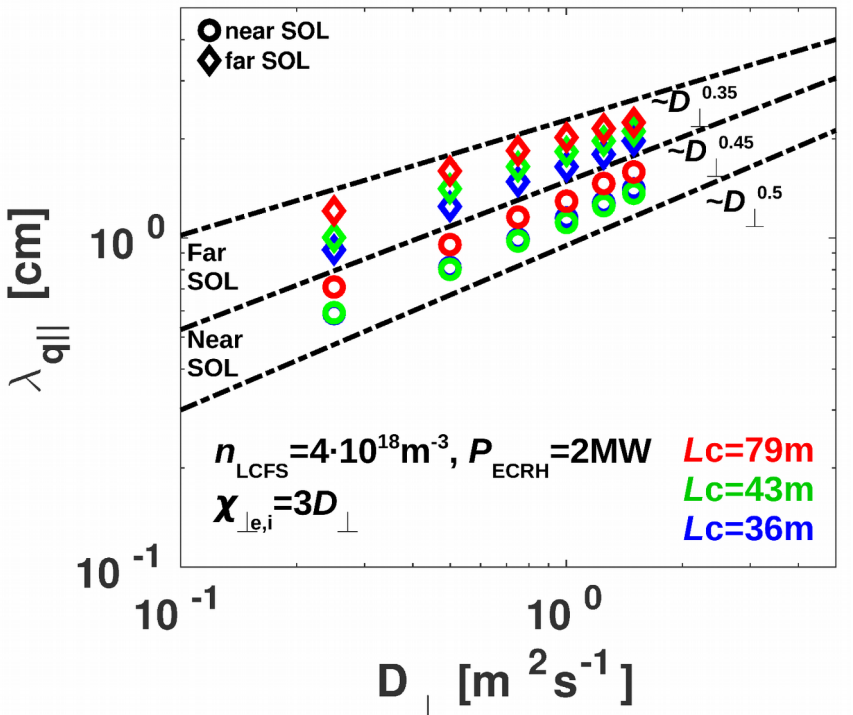
Near and far SOL identified in heat flux profile with dependence of heat flux on L_c



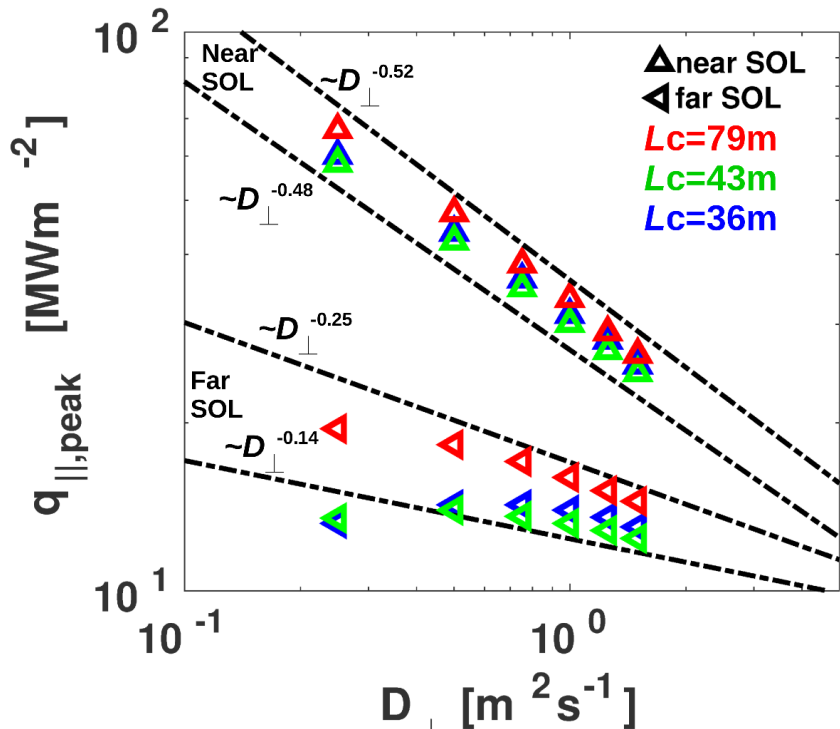
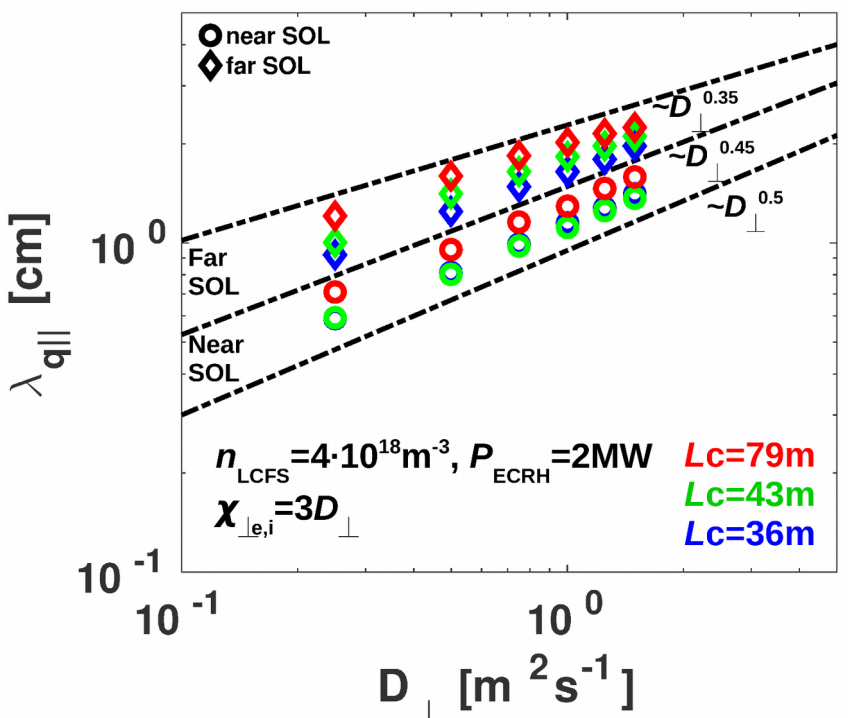
Heat flux characteristics
($\lambda_{q_{\parallel},\text{near,far}}$, $q_{\text{peak},\text{near,far}}$) for
near and far SOL for
long and short L_c

How does \perp (anomalous)
transport affect q_{\parallel} ?

Near SOL power width and peak power follow mostly simple SOL scaling $\sim D_{\perp}^{\pm 0.5}$

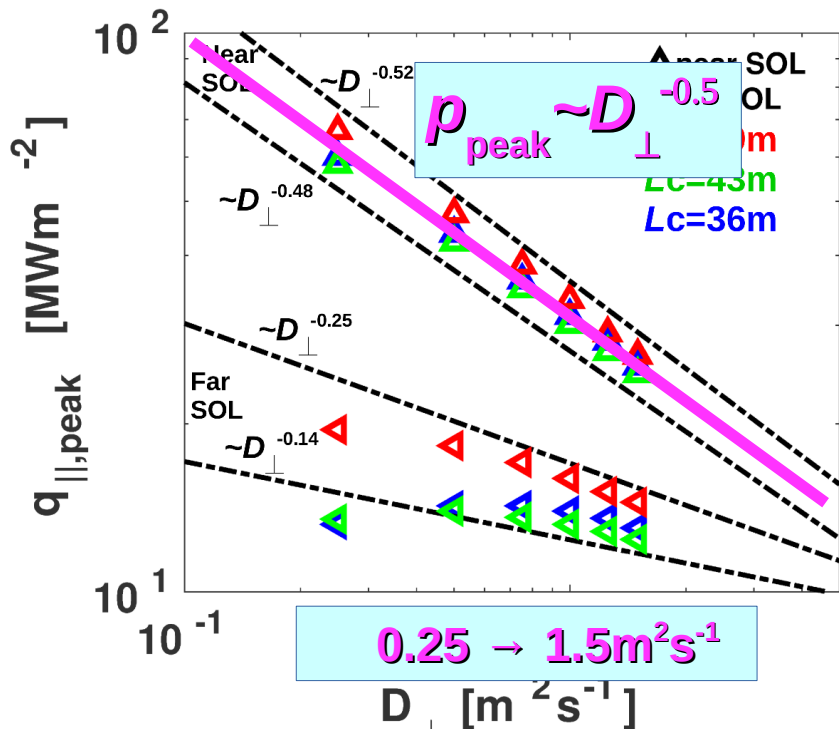
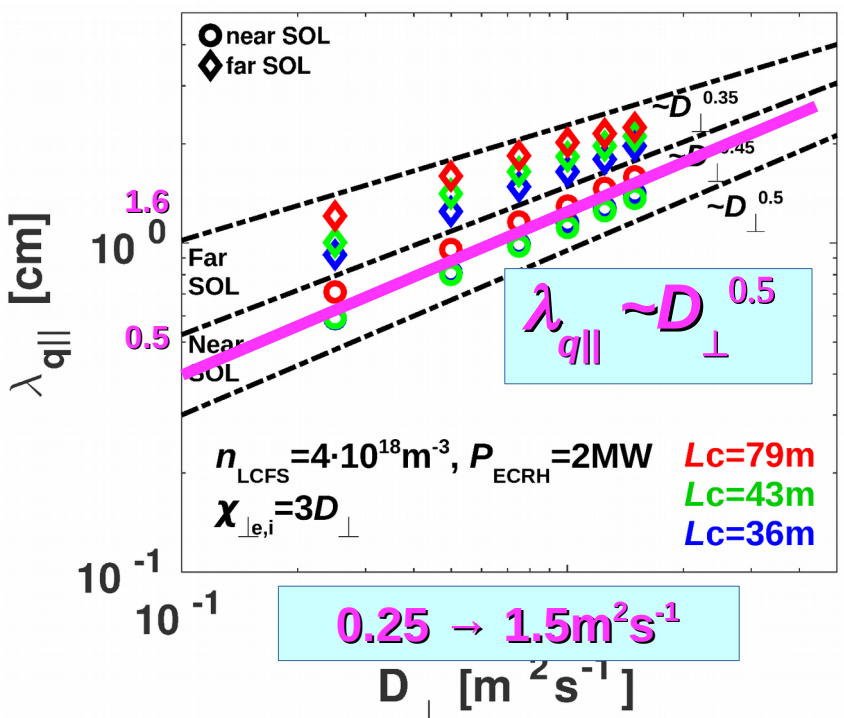


Near SOL power width and peak power follow mostly simple SOL scaling $\sim D_{\perp}^{\pm 0.5}$

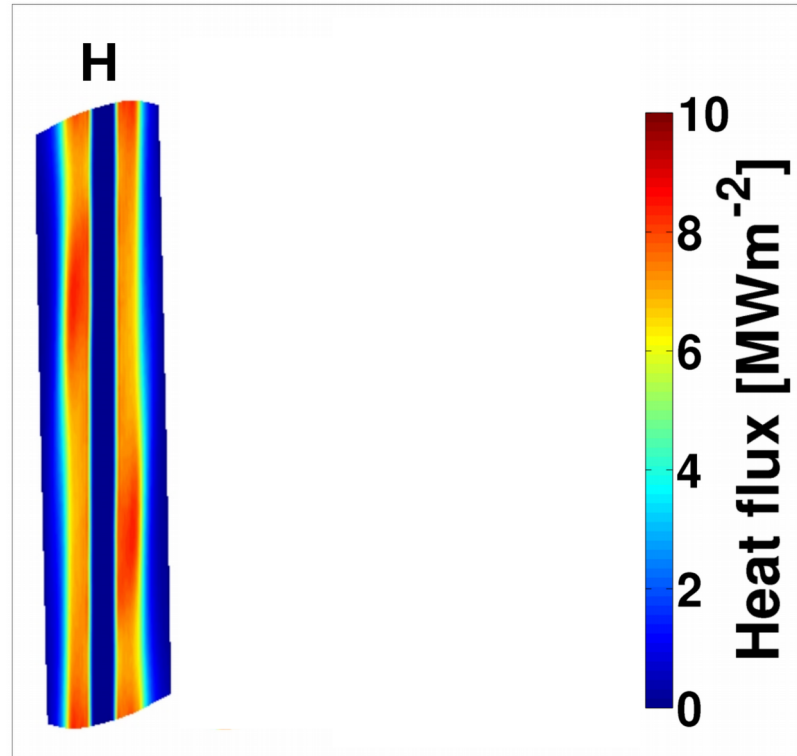


F. Effenberg, Y. Feng et al., IAEA, 2016

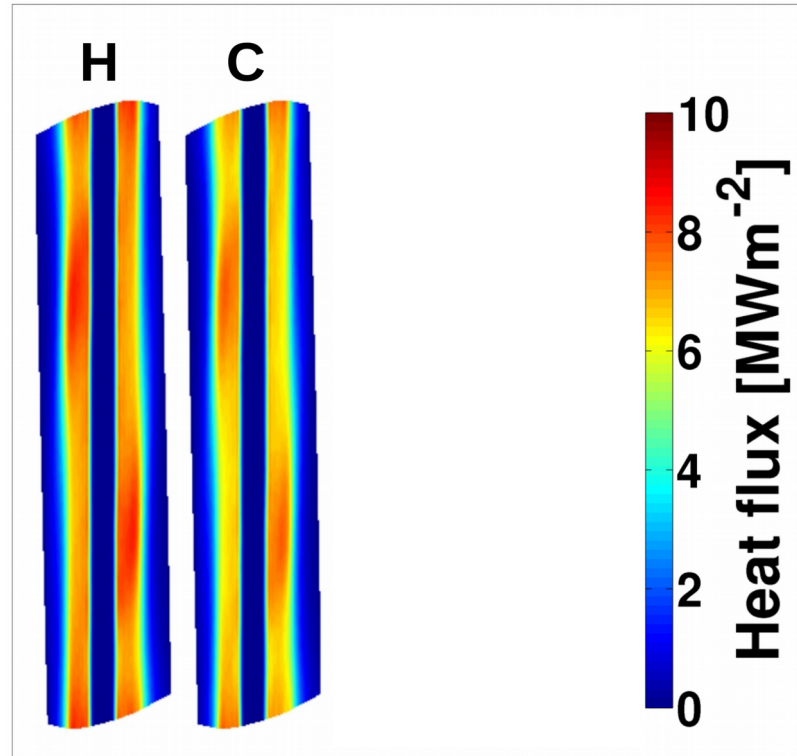
Near SOL power width and peak power follow mostly simple SOL scaling $\sim D_{\perp}^{\pm 0.5}$



Feasibility of heat flux mitigation by radiative edge cooling predicted by 3-D modeling

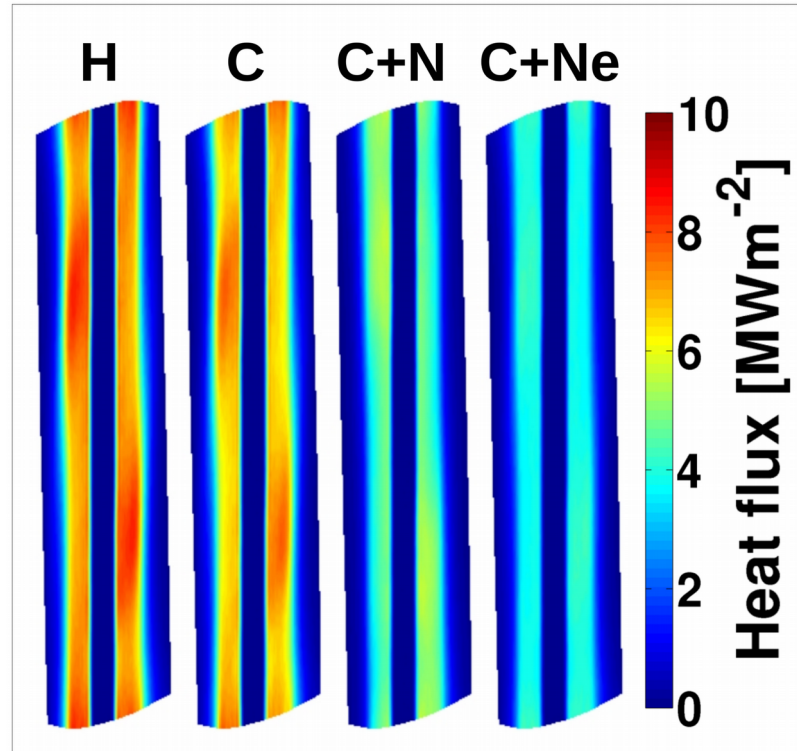
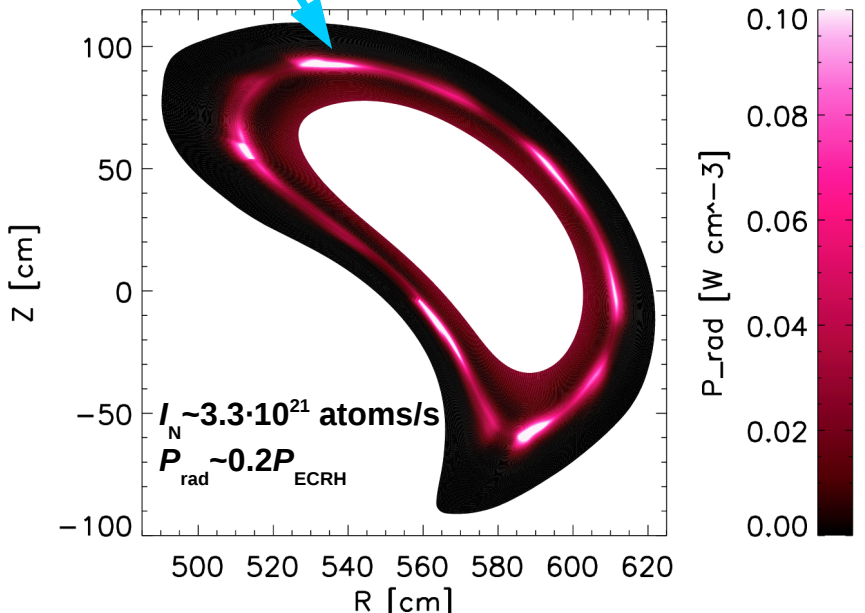


Feasibility of heat flux mitigation by radiative edge cooling predicted by 3-D modeling



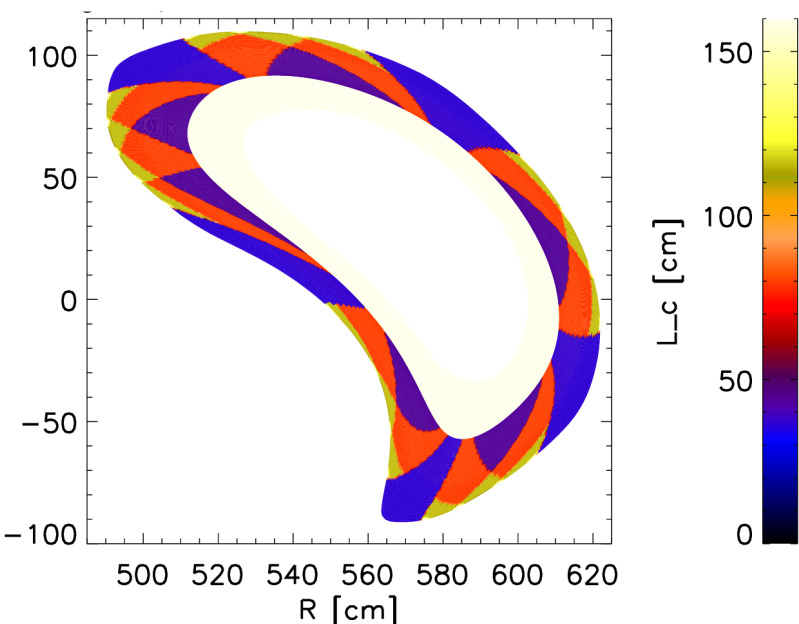
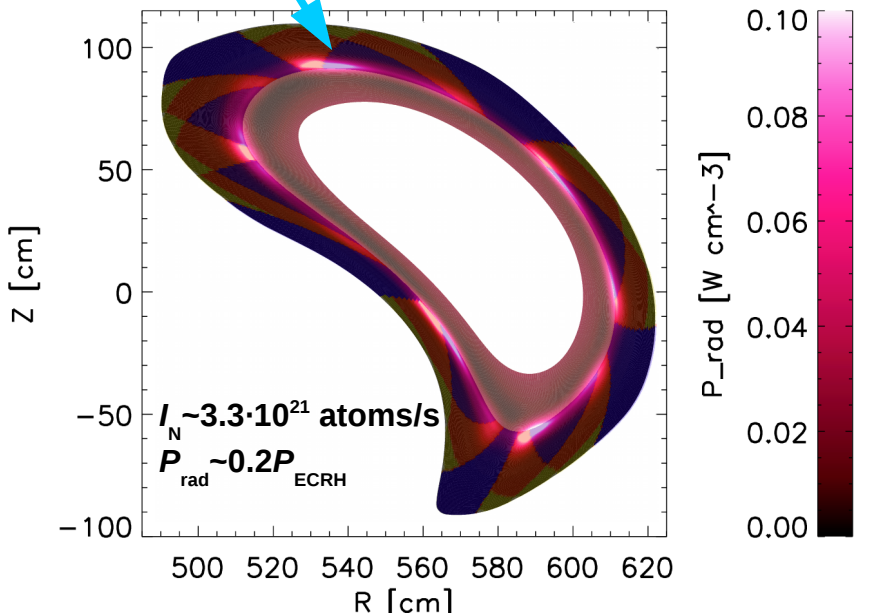
Feasibility of heat flux mitigation by radiative edge cooling predicted by 3-D modeling

N injection



Feasibility of heat flux mitigation by radiative edge cooling predicted by 3-D modeling

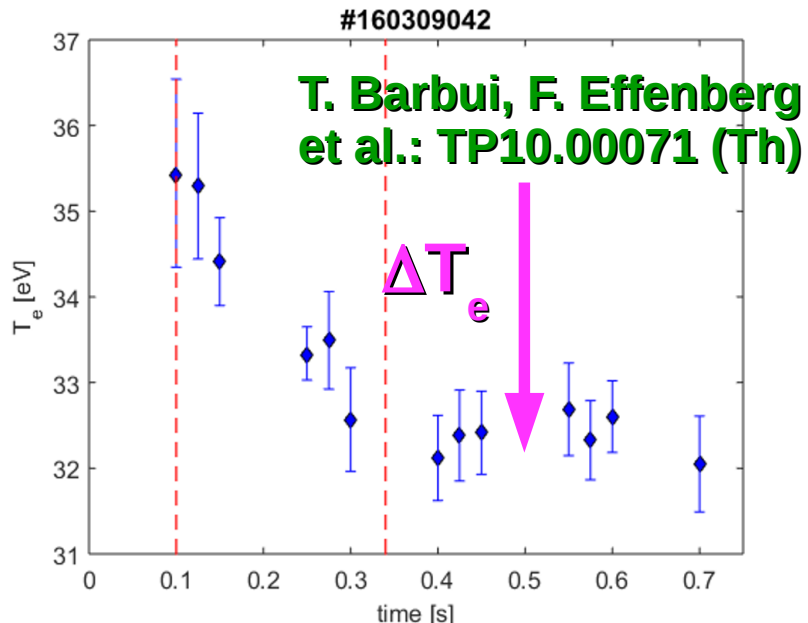
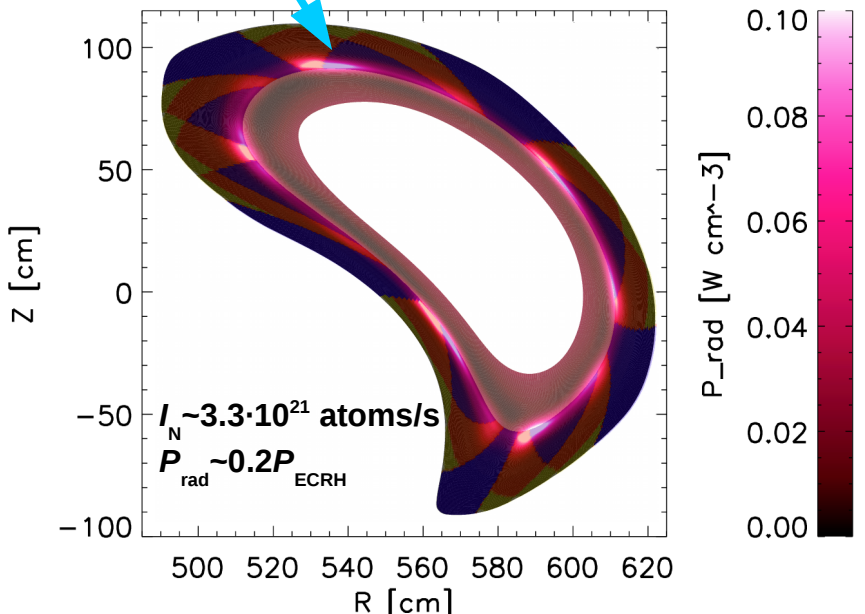
N injection



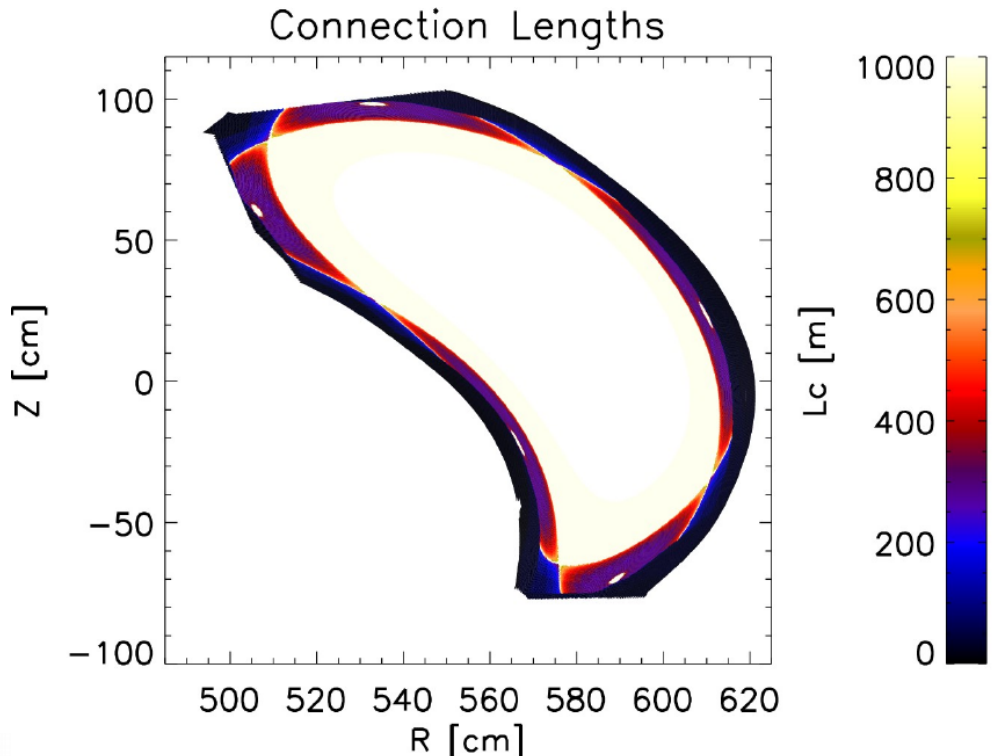
Radiation peaks in longer flux tubes

Feasibility of heat flux mitigation by radiative edge cooling predicted by 3-D modeling

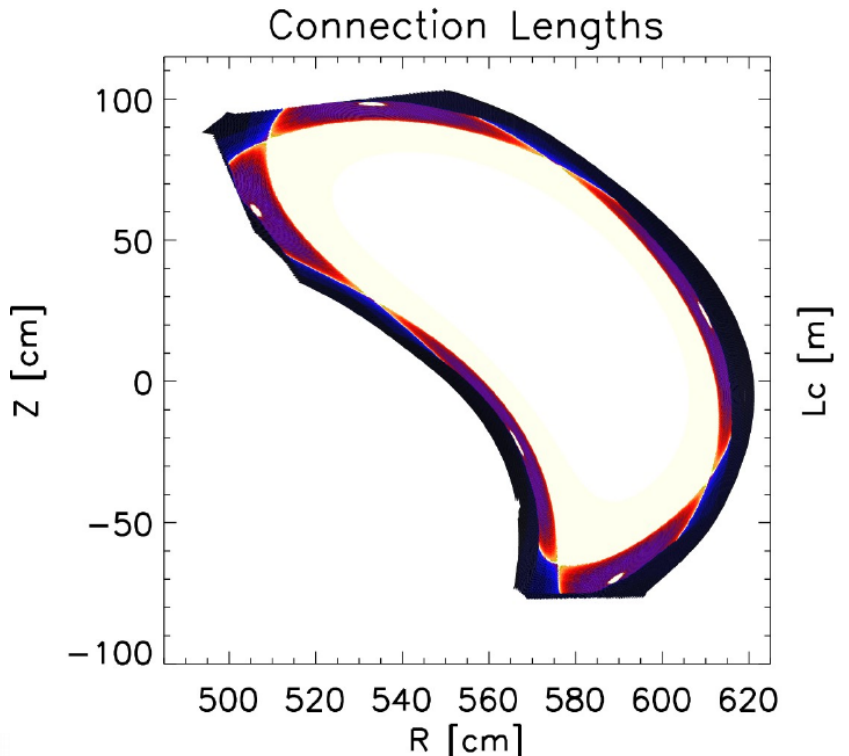
N injection



Exploration of heat flux mitigation by impurity seeding for island divertor phase is ongoing

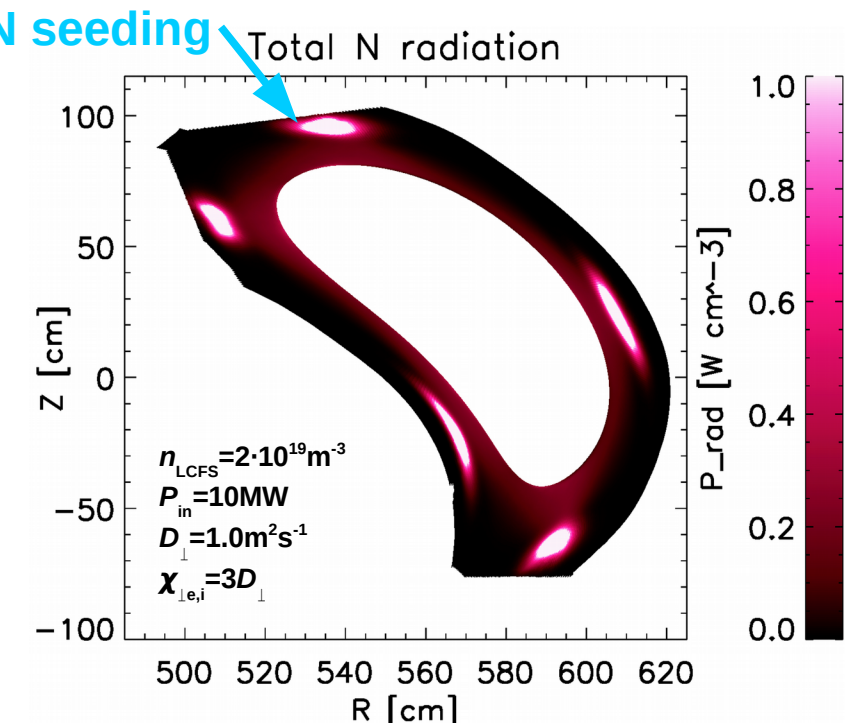
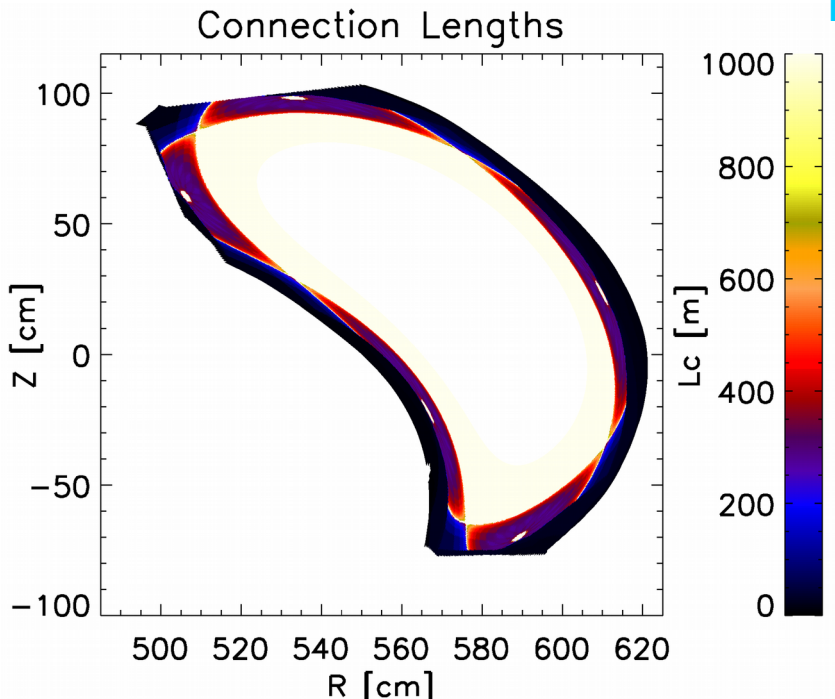


Exploration of heat flux mitigation by impurity seeding for island divertor phase is ongoing

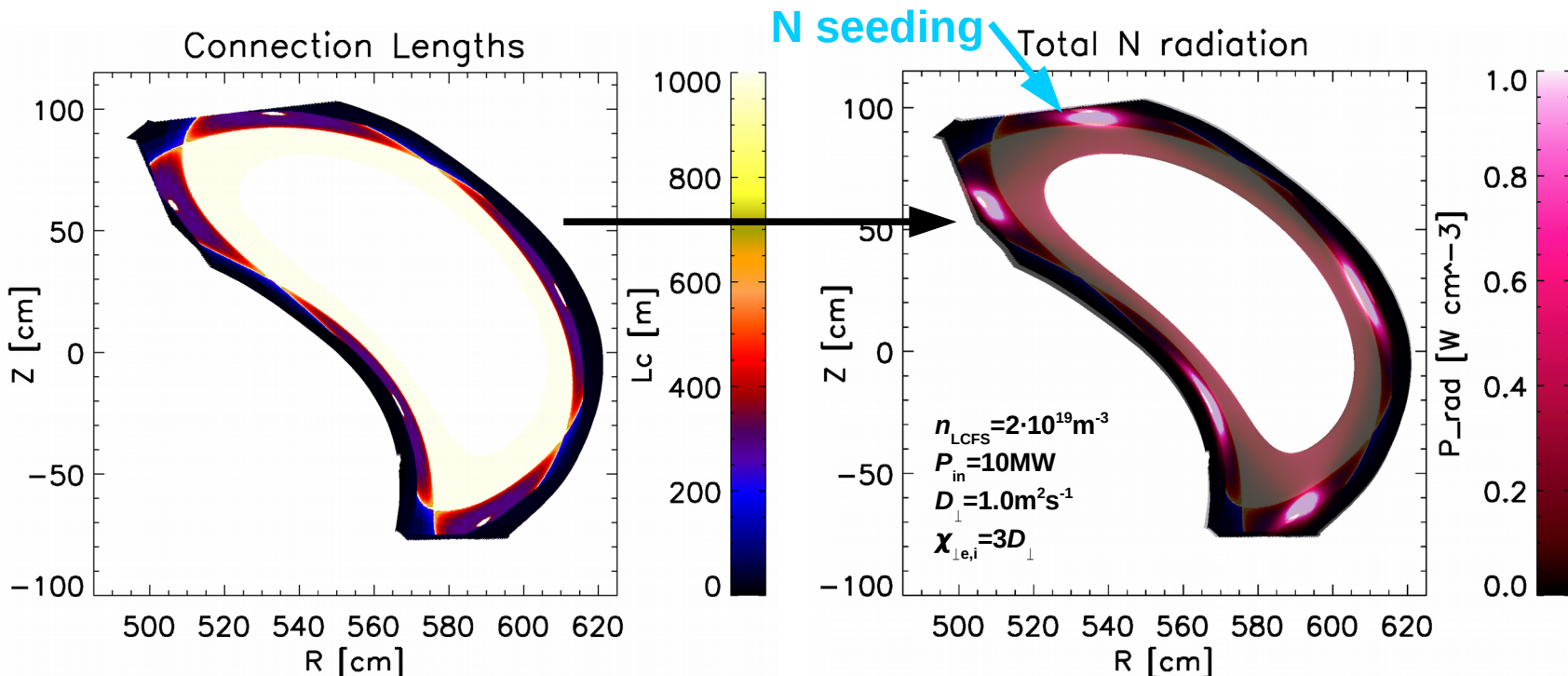


→ L_c increase by
a factor ~10

Exploration of heat flux mitigation by impurity seeding for island divertor phase is ongoing

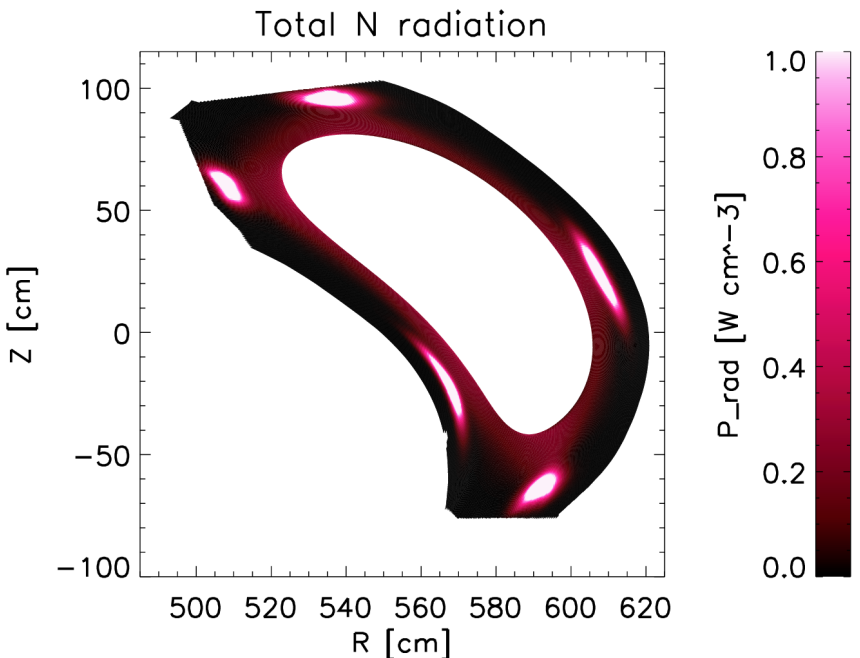


Exploration of heat flux mitigation by impurity seeding for island divertor phase is ongoing



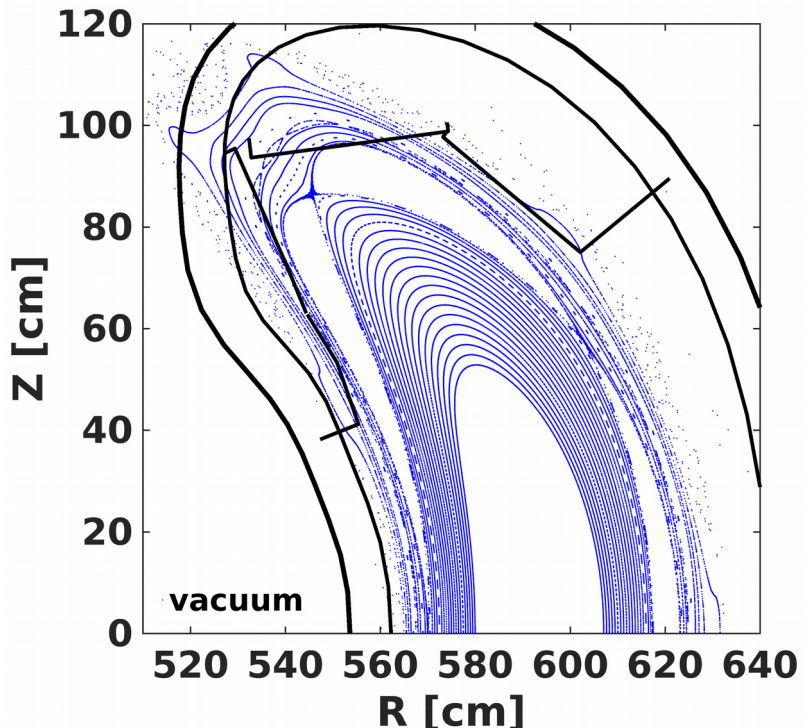
Radiating islands

Initial modeling shows accumulation of N injected inside of island divertor domain

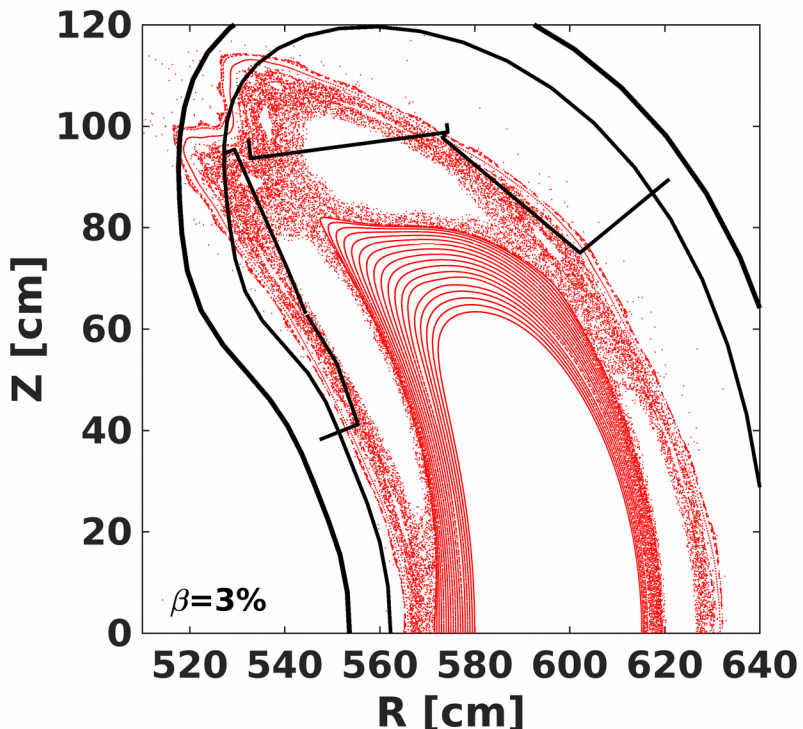
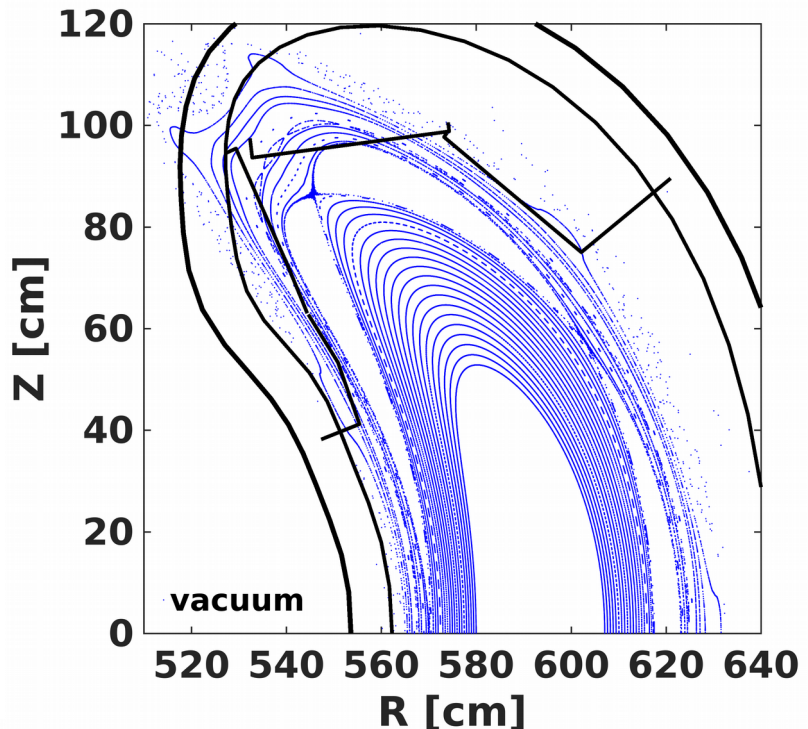


Radiating islands potentially beneficial for cooling

High performance operation: how will beta effects affect heat transport and edge cooling? HINT2 → EMC3-EIRENE



High performance operation: how will beta effects affect heat transport and edge cooling? HINT2 → EMC3-EIRENE



(HINT2 equilibrium: courtesy of Y. Suzuki)

Conclusion

- Limiter heat fluxes correlated to L_c , confirmed by IR
- Heat flux characteristics: near and far SOL regime
- \perp transport: q_{peak} and λ_{qll} scale for different L_c almost simple SOL like in near SOL
- Comparison with experimental results is ongoing
- Radiative edge cooling tested during limiter phase, preparation for Island divertor is in progress

Contributions related to this study

O. Schmitz et al.: TP10.00072 (Th)

T. Sunn Pedersen et al.: AR1.00001 (Mo)

G. Wurden, H. Niemann et al.: CP10.00054 (Mo)

T. Barbui, F. Effenberg et al.: TP10.00071 (Th)

H. Frerichs, F. Effenberg et al.: TP10.00074 (Th)

L. Stephey, F. Effenberg et al.: JI3.00001 (Tu)

V. Winters, C. Biedermann et al.: TP10.00073 (Th)

more
results
Thursday
morning

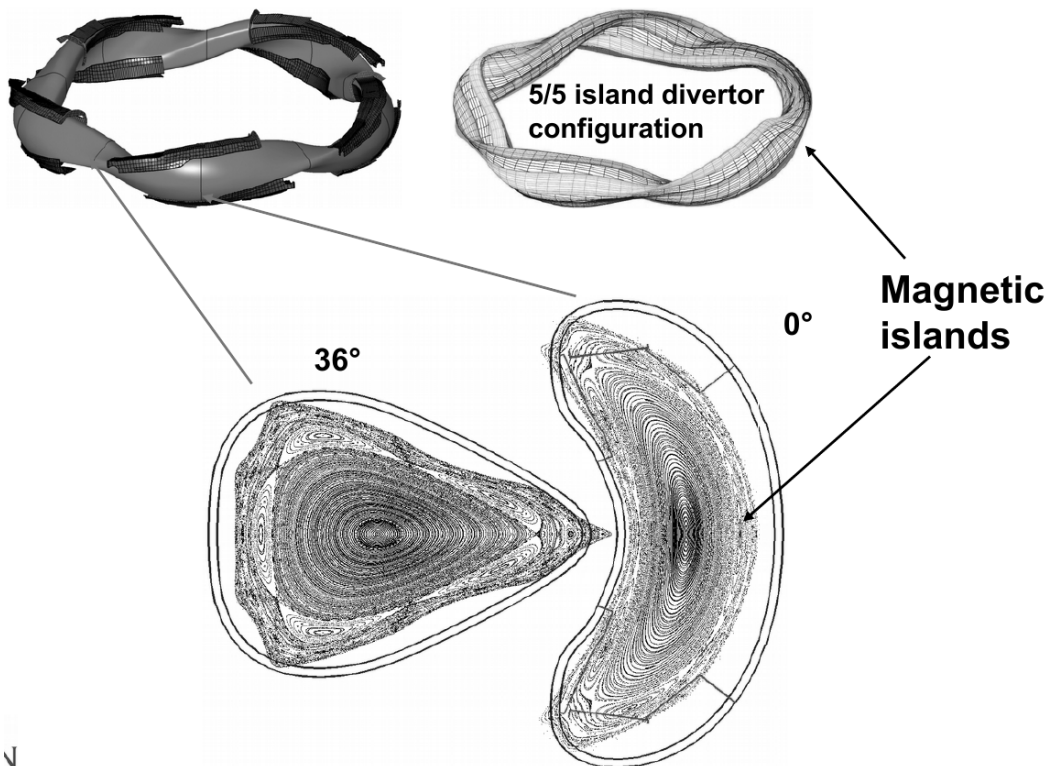


Acknowledgments (HPC):

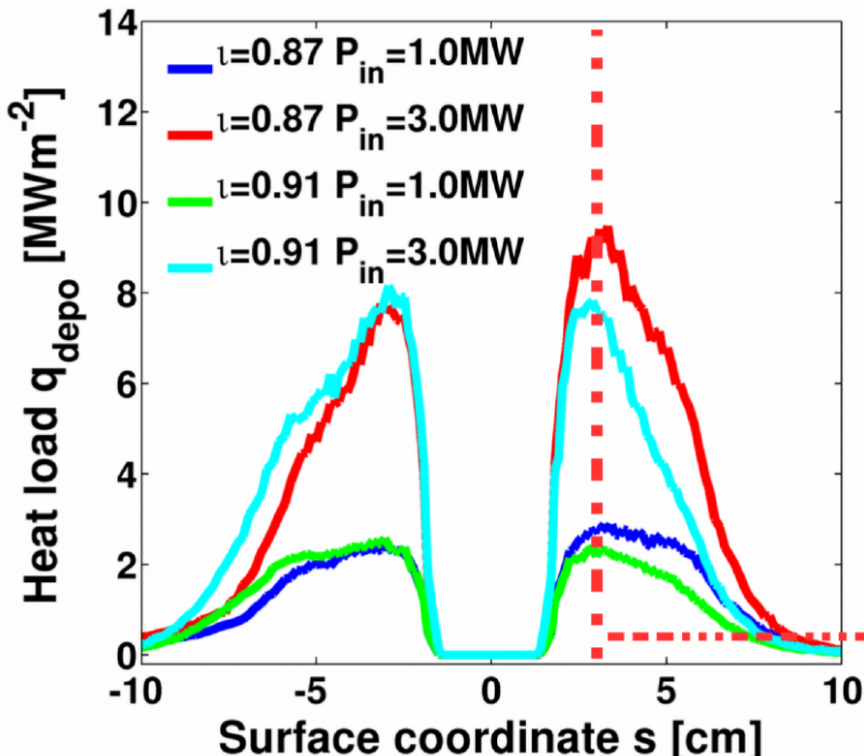
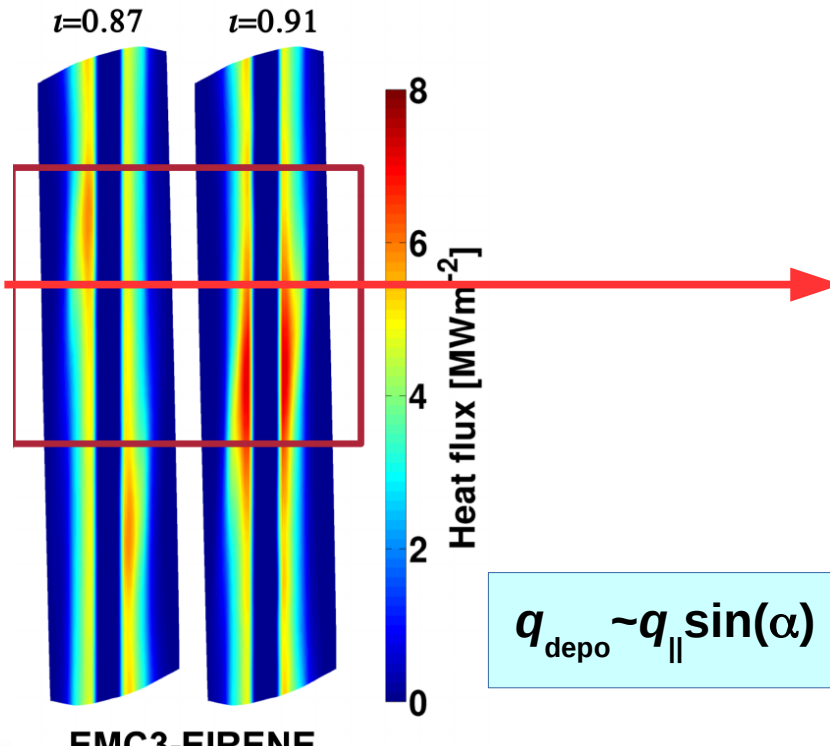
This research was performed using the computer resources and assistance of the UW-Madison **Center For High Throughput Computing (CHTC)** and the high performance computing system **"Hydra"** of the **Max-Planck-Society** at **Rechenzentrum Garching (RZG)**.

APPENDIX

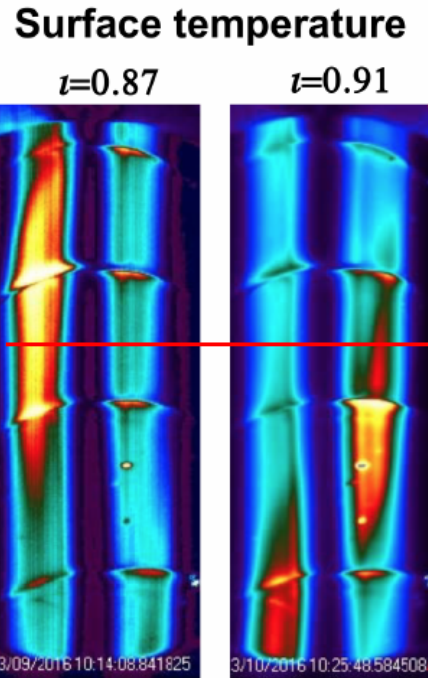
Island divertor configuration



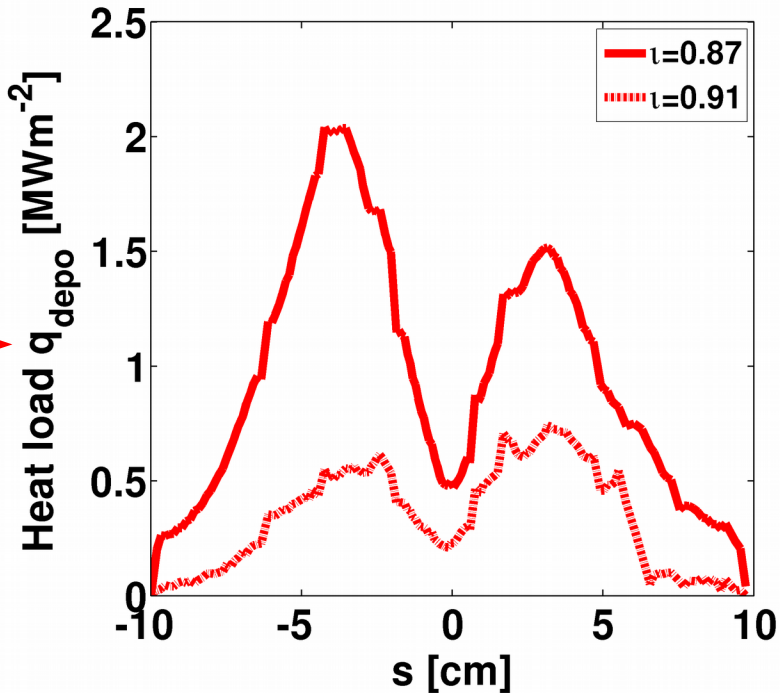
Issue for heat flux analysis: target heat loads strongly modified by target geometry function



3-D modeling now used to interpret heat fluxes inferred from IR thermography for different iota configurations



THEODOR Code [2]:
 $T_{\text{surf}} [\text{C}] \rightarrow q_{\text{depo}} [\text{Wm}^2]$

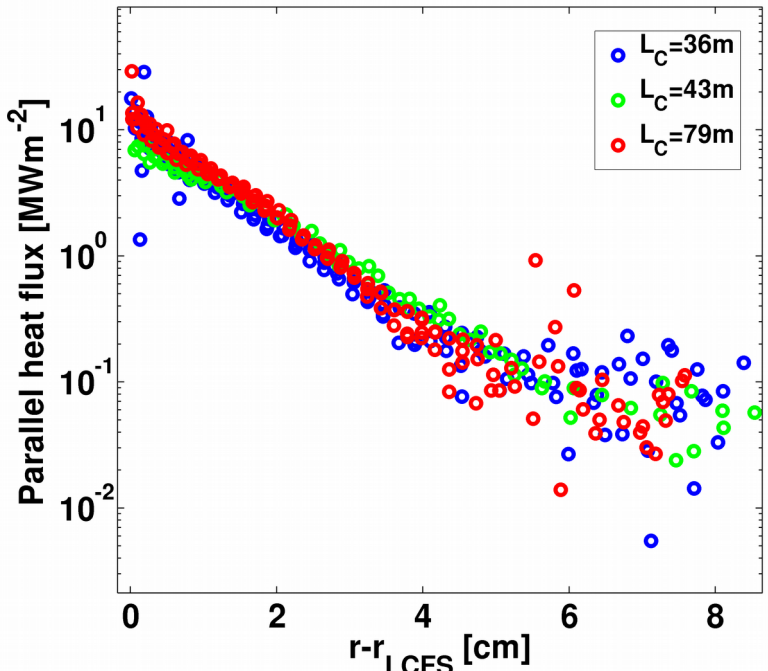


IR Thermography

[2] B. Sieglin, M. Faitsch, A. Hermann et al.,
Review of Scientific Instruments, 86, 113502 (2015)

Data courtesy of G.A. Wurden &
H. Niemann

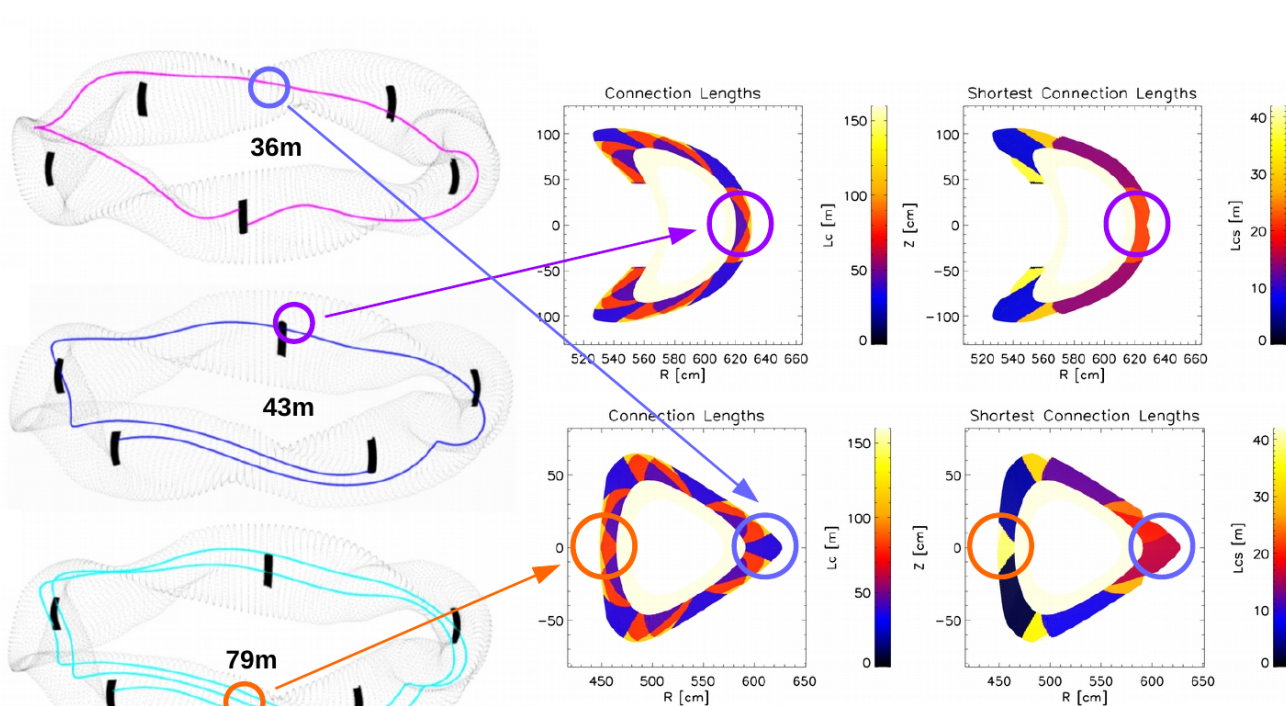
3-D modeling now used to interpret heat fluxes inferred from IR thermography for different iota configurations



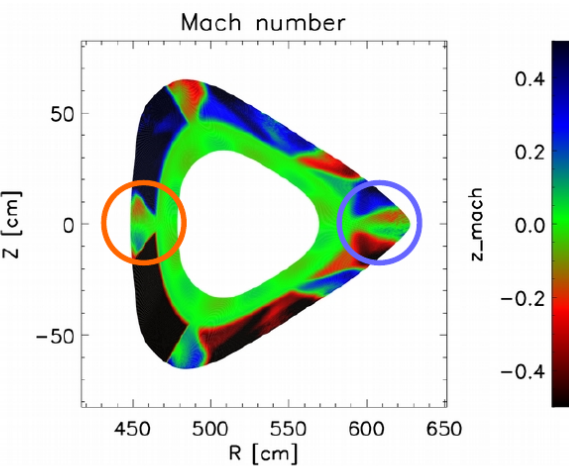
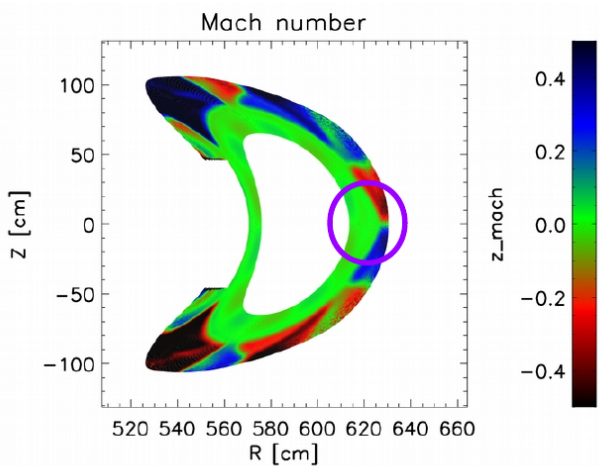
$$\lambda_{q||} \sim 1.0\text{-}1.4\text{cm}$$

Local measurement!
(→ error fields,
transient behavior,
impurity mix)

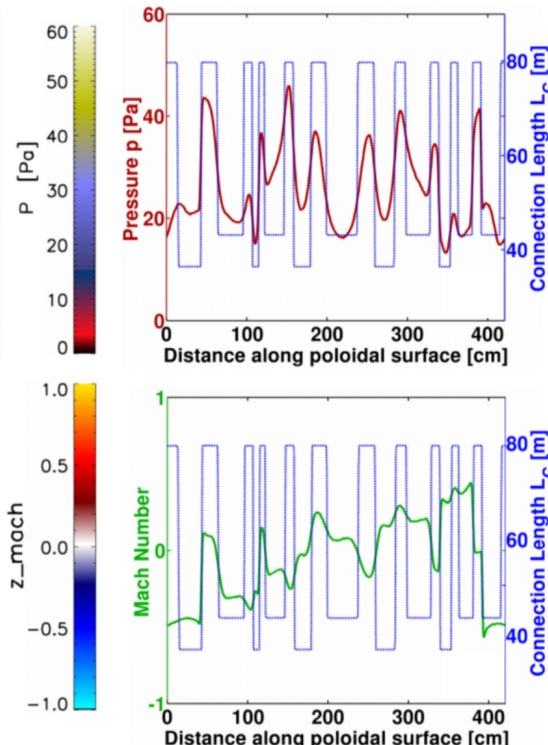
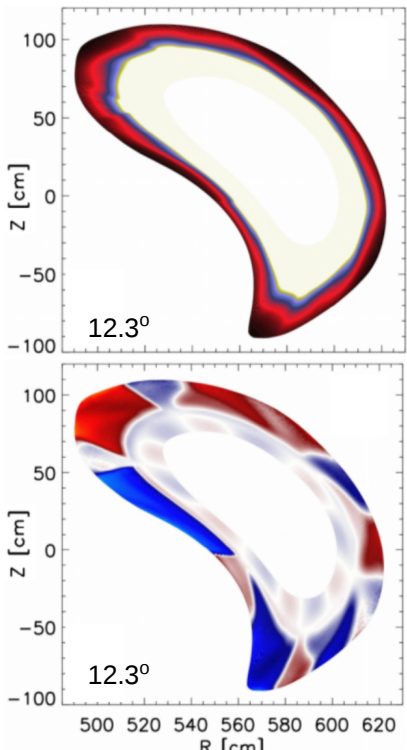
How are upstream positions defined?



Stagnation points



Plasma pressure is modulated in correlation to L_c and drives counter streaming flows

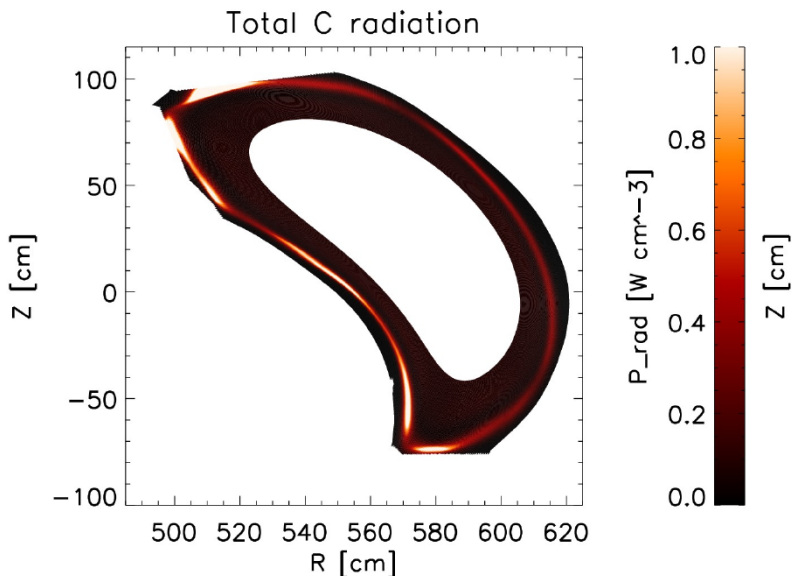


1-D poloidal scan:
 $p(\theta_{\text{pol}}) \sim L_c(\theta_{\text{pol}})$

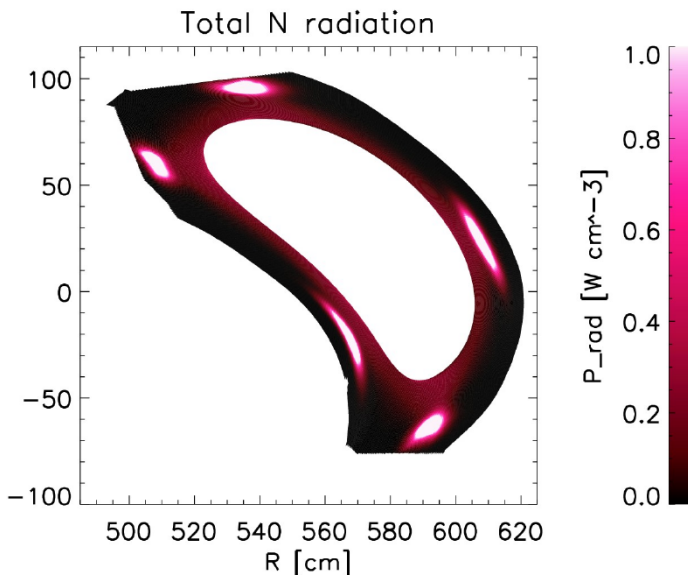
Flow patterns depend on L_c and shortest distance to target $L_{c,\text{shortest}}$

Initial modeling shows accumulation of N injected inside of island divertor domain

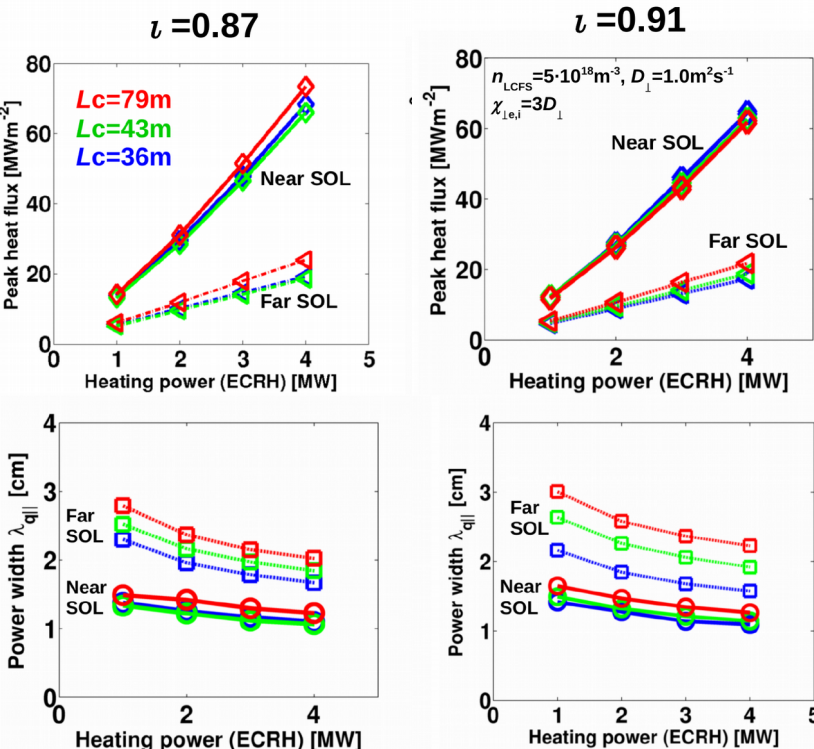
Cooling and detachment
based on intrinsic carbon?



Impurity seeding →
radiating islands



Strong linear dependence of heat flux level on P_{ECRH}



The edge transport model

Particle balance

$$\nabla \cdot [n_i u_{\parallel} \mathbf{e}_{\parallel} - D_{\perp} \mathbf{I}_{\perp} \cdot \nabla n_i] = S_p. \quad (\text{A1})$$

Parallel momentum balance

$$\begin{aligned} & \nabla \cdot \mathbf{e}_{\parallel} [m_i n_i u_{\parallel}^2 - \eta \mathbf{e}_{\parallel} \cdot \nabla u_{\parallel}] - \nabla \cdot \mathbf{I}_{\perp} \cdot D_{\perp} \nabla (m_i n_i u_{\parallel}) \\ &= -\mathbf{e}_{\parallel} \cdot \nabla p + S_m. \end{aligned} \quad (\text{A2})$$

Energy balance (electrons and ions)

$$\begin{aligned} & \nabla \cdot \mathbf{e}_{\parallel} \left[\frac{5}{2} T_e n_i u_{\parallel} - \kappa_e \mathbf{e}_{\parallel} \cdot \nabla T_e \right] \\ & - \nabla \cdot \mathbf{I}_{\perp} \cdot \left[\chi_e n_i \nabla T_e + \frac{5}{2} T_e D_{\perp} \nabla n_i \right] = -k(T_e - T_i) + S_{ee}, \end{aligned} \quad (\text{A3})$$

$$\begin{aligned} & \nabla \cdot \mathbf{e}_{\parallel} \left[\frac{5}{2} T_i n_i u_{\parallel} - \kappa_i \mathbf{e}_{\parallel} \cdot \nabla T_i \right] \\ & - \nabla \cdot \mathbf{I}_{\perp} \cdot \left[\chi_i n_i \nabla T_i + \frac{5}{2} T_i D_{\perp} \nabla n_i \right] = +k(T_e - T_i) + S_{ei}. \end{aligned} \quad (\text{A4})$$

Equations taken from: H. Frerichs et al.,
Physics of Plasmas 22, 072508 (2015)